TECHNICAL REPORT ARBRL-TR-02358

COMPUTATIONAL PARAMETRIC STUDY OF THE AERODYNAMICS OF SPINNING SLENDER BODIES AT SUPERSONIC SPEEDS

W. B. Sturek
D. C. Mylin
C. C. Bush

August 1981

US ARMY ARMAMENT RESEARCH AND DEVELOPMENT COMMAND
BALLISTIC RESEARCH LABORATORY
ABERDEEN PROVING GROUND, MARYLAND

Destroy this report when it is no longer needed.
Do not return it to the originator.

Secondary distribution of this report by originating or sponsoring activity is prohibited.

Additional copies of this report may be obtained from the National Technical Information Service, U.S. Department of Commerce, Springfield, Virginia 22161.

The findings in this report are not to be construed as an official Department of the Army position, unless so designated by other authorized documents.

The use of trade names or manufacturers' names in this report does not constitute indorsement of any commercial product.

UNCLASSIFIED

SECURITY CLASSIFICATION OF THIS PAGE *(When Data Entered)*

REPORT DOCUMENTATION PAGE		READ INSTRUCTIONS BEFORE COMPLETING FORM
1. REPORT NUMBER TECHNICAL REPORT ARBRL-TR-02358	2. GOVT ACCESSION NO.	3. RECIPIENT'S CATALOG NUMBER
4. TITLE *(and Subtitle)* Computational Parametric Study of the Aerodynamics of Spinning Slender Bodies at Supersonic Speeds		5. TYPE OF REPORT & PERIOD COVERED Final 6. PERFORMING ORG. REPORT NUMBER
7. AUTHOR*(s)* W.B. Sturek, D.C. Mylin, and C.C. Bush		8. CONTRACT OR GRANT NUMBER*(s)*
9. PERFORMING ORGANIZATION NAME AND ADDRESS U.S. Army Ballistic Research Laboratory (ATTN: DRDAR-BLL) Aberdeen Proving Ground, Maryland 21005		10. PROGRAM ELEMENT, PROJECT, TASK AREA & WORK UNIT NUMBERS RDT&E 1L162618AH80
11. CONTROLLING OFFICE NAME AND ADDRESS US Army Armament Research & Development Command US Army Ballistic Research Laboratory (DRDAR-BL) Aberdeen Proving Ground, MD 21005		12. REPORT DATE AUGUST 1981 13. NUMBER OF PAGES 39
14. MONITORING AGENCY NAME & ADDRESS*(if different from Controlling Office)*		15. SECURITY CLASS. *(of this report)* Unclassified 15a. DECLASSIFICATION/DOWNGRADING SCHEDULE

16. DISTRIBUTION STATEMENT *(of this Report)*

Approved for public release; distribution unlimited.

17. DISTRIBUTION STATEMENT *(of the abstract entered in Block 20, if different from Report)*

18. SUPPLEMENTARY NOTES

19. KEY WORDS *(Continue on reverse side if necessary and identify by block number)*

Projectile aerodynamics
Supersonic flow
Finite difference computations

20. ABSTRACT *(Continue on reverse side if necessary and identify by block number)*

Three dimensional finite-difference flow field computation techniques have been employed to generate a parametric aerodynamic study at supersonic speeds. Computations for viscous turbulent and inviscid flow have been performed for cone-cylinder, secant-ogive-cylinder, and tangent-ogive-cylinder bodies for a Mach number range of $1.75 \leq M \leq 5$. The aerodynamic coefficients computed are pitching moment, normal force, center of pressure, Magnus moment, Magnus force, Magnus center of pressure, form drag, viscous drag, roll damping and pitch damping. All aerodynamic coefficients are computed in a

DD FORM 1 JAN 73 1473 EDITION OF 1 NOV 65 IS OBSOLETE

UNCLASSIFIED

SECURITY CLASSIFICATION OF THIS PAGE *(When Data Entered)*

20. ABSTRACT (Continued)

conceptually exact manner. The only empirical input is that required for turbulence modeling. Computed results are compared to experimental data from free flight aerodynamic ranges and wind tunnels in order to validate the computational techniques. Parametric comparisons illustrate the effects of body configuration and Mach number for the ten aerodynamic coefficients. The results for Magnus and pitch damping are of particular interest.

TABLE OF CONTENTS

LIST OF ILLUSTRATIONS

LIST OF ILLUSTRATIONS
(Continued)

I. INTRODUCTION

Recent trends in projectile design have led to shapes with greater length and more slender ogives. Unexpected flight stability problems have been encountered due to decreased aerodynamic stability of these new shapes. Clearly, conventional aerodynamic predictive capabilities were not adquate. In an effort to avoid these problems in the future, the Ballistic Research Laboratory has been developing advanced numerical computational techniques for computing projectile aerodynamic characteristics to improve shell design technology.

Substantial progress has been made in the past 10 years in the development of aerodynamic computational techniques and in the availability of high speed digital computers. This progress has made it possible to begin to use advanced finite-difference computational techniques to perform parametric aerodynamic studies for evaluation of proposed design concepts.

The use of advanced numerical computational techniques for a parametric study is difficult to justify to compute only static aerodynamic parameters since cheaper, less complex techniques such as Ref. (1), (2) and (3) are available. However, if dynamic derivatives such as Magnus and pitch damping are considered important and if viscous drag is of interest, then the advanced computational techniques are justified and, in fact, must be used. This paper reports the initial results of an ongoing research effort at BRL to form an advanced aerodynamic computation capability that will provide the shell designer with a complete package of static and dynamic aerodynamic coefficients for use in design studies.

II. COMPUTATIONAL TECHNIQUES

A. Scope of Effort

Three dimensional finite-difference flow field computational techniques for inviscid and turbulent viscous flow have been applied to generate a comprehensive set of aerodynamic coefficients for cone-cylinder (CC), tangent-ogive-cylinder (TOC), and secant-ogive-cylinder (SOC) body configurations. The model geometries considered in this study are shown in Figure 1. Body lengths up to seven calibers and ogive lengths of two, three, and four calibers have been considered. The aerodynamic coefficients computed are pitching

---

1. *Whyte, R., "SPIN-73, An Updated Version of the Spinner Computer Program," Picatinny Arsenal Technical Report 4588, November 1973.*

2. *Moore, F.G. and McKerley, C.W., "Aerodynamics of Guided and Unguided Weapons; Part II - Computer Program and Usage", NWL TR-3036, 1974.*

3. *Moore, F.G. and Swanson, R.C., "Aerodynamics of Tactical Weapons to Mach Number 3 and Angle of Attack 15°, Part I - Theory and Application", NSWC/DL TR-3584, February 1977.*

moment, normal force, center of pressure, Magnus moment, Magnus force, Magnus center of pressure, form and viscous drag, roll damping and pitch damping. The sign convention for the pitch plane and Magnus forces is shown in Figure 2. All aerodynamic coefficients are computed in a conceptually exact manner. The only empirical input is that required for the modeling of turbulent eddy viscosity.

The computations have been carried out for a Mach number range of $1.75 \leq M \leq 5$. These computations were all performed for an angle of attack of 1°, a nondimensional spin rate (PD/V) of 0.19, and for sea level atmospheric free-stream conditions. Specific comparisons to wind tunnel data were made for the tunnel operating conditions.

B. Coupled Inviscid-Viscous Computations

The sequence of computations which are run in order to compute the static aerodynamic parameters, including turbulent viscous effects, is shown in Figure 3. Each block represents a separate computer code. These codes have been combined using the overlay technique on the BRL Cyber computer. The two main codes are those which compute three dimensional turbulent boundary layer development and three dimensional inviscid flow.

The computation of the effects of viscosity is of crucial importance when such parameters as roll damping, Magnus, and drag are of interest. The technique employed here is a fully implicit, finite difference numerical scheme developed by Dwyer[4] . This technique takes into consideration the changes in direction of the cross-flow velocity that occur on the side of the shell where the inviscid cross-flow opposes the surface spin.

The equations of motion solved are the basic equations defining the three-dimensional compressible, turbulent boundary-layer flow over a body of revolution described by the relation $r = r(x)$. The coordinate system is shown in Figure 4.

Continuity

$$\frac{\partial}{\partial x}(r\bar{\rho}\bar{u}) + \frac{\partial}{\partial y}(r\bar{\rho}v) + \frac{\partial}{\partial \phi}(\bar{\rho}\bar{w}) = 0 \tag{1}$$

x momentum

$$\bar{\rho}\left[\bar{u}\frac{\partial \bar{u}}{\partial x} + v\frac{\partial \bar{u}}{\partial y} + \frac{\bar{w}}{r}\frac{\partial \bar{u}}{\partial \phi} - \frac{\bar{w}^2}{r}\frac{\partial r}{\partial x}\right] =$$

$$-\frac{\partial \bar{p}_e}{\partial x} + \frac{\partial}{\partial y}\left[\mu\frac{\partial \bar{u}}{\partial y} - \overline{\rho u' v'}\right] \tag{2}$$

---

4. *Dwyer, H.A. and Sanders, B.R., "Magnus Forces on Spinning Supersonic Cones. Part I: The Boundary Layer", AIAA Journal, Vol. 14, April 1976, pp. 498-504.*

ϕ momentum

$$\bar{\rho}\left[\bar{u}\frac{\partial \bar{w}}{\partial x} + v\frac{\partial \bar{w}}{\partial y} + \frac{\bar{w}}{r}\frac{\partial \bar{w}}{\partial \phi} + \frac{\bar{u}\bar{w}}{r}\frac{\partial r}{\partial x}\right] = -\frac{1}{r}\frac{\partial \bar{p}_e}{\partial \phi} + \frac{\partial}{\partial y}\left[\mu\frac{\partial \bar{w}}{\partial y} - \overline{\rho v' w'}\right] \tag{3}$$

Energy

$$\bar{\rho}\left[\bar{u}\frac{\partial \bar{h}}{\partial x} + v\frac{\partial \bar{h}}{\partial y} + \frac{\bar{w}}{r}\frac{\partial \bar{h}}{\partial \phi}\right] = \bar{u}\frac{\partial \bar{p}_e}{\partial w} + \frac{\bar{w}}{r}\frac{\partial \bar{p}_e}{\partial \phi}$$

$$+ \mu\left[\left(\frac{\partial \bar{u}}{\partial y}\right)^2 + \left(\frac{\partial \bar{w}}{\partial y}\right)^2\right] - \overline{\rho u' v'}\frac{\partial \bar{u}}{\partial y} - \overline{\rho v' w'}\frac{\partial \bar{w}}{\partial y} \tag{4}$$

$$+ \frac{\partial}{\partial y}\left[\frac{\mu}{Pr}\frac{\partial \bar{h}}{\partial y} - \overline{\rho v' h'}\right]$$

where $v = \bar{v} + \overline{\rho' v'}/\bar{\rho}$ and the bar indicates a time-averaged quantity.

In order to obtain closure of this system of equations, the following models of the turbulence terms have been introduced:

Turbulent shear stress

$$-\overline{\rho u' v'} = -\overline{\rho v' w'} = \bar{\rho}\ell^2\left[\left(\frac{\partial \bar{u}}{\partial y}\right)^2 + \left(\frac{\partial \bar{w}}{\partial y}\right)^2\right] =$$

$$\varepsilon\left[\left(\frac{\partial \bar{u}}{\partial y}\right)^2 + \left(\frac{\partial \bar{w}}{\partial y}\right)^2\right]^{1/2}$$

where ε is introduced as the turbulent viscosity and the mixing length, $\ell = 0.09\,\delta \tanh\left[(0.4/0.09)(y/\delta)\right]$. Van Driest damping is used to account for the effect of the laminar sublayer.

Turbulent heat transfer

$$-\overline{\rho v' h'} = \frac{k_t}{c_p}\frac{\partial \bar{h}}{\partial y}$$

The turbulent Prandtl number is introduced as

$$Pr_t = c_p \varepsilon / k_t = 0.90$$

The three-dimensional displacement surface is not merely the vector sum of the longitudinal and circumferential components of the boundary-layer displacement thickness. Instead, the differential equation derived by Moore[5]:

---

5. *Moore, F.N., "Displacement Effect of a Three-Dimensional Boundary Layer", NACA TN 2722. June 1952.*

$$\frac{\partial}{\partial x}\left[\rho_e u_e r(\delta^*_{3D}-\delta^*_x)\right] + \frac{\partial}{\partial \phi}\left[\rho_e w_e(\delta^*_{3D}-\delta^*_\phi)\right] = 0 \qquad (5)$$

must be solved for δ^*_{3D}, the three-dimensional boundary-layer displacement thickness where

$$\delta^*_x = \int_0^\delta \left(1 - \frac{\rho u}{\rho_e u_e}\right)dy$$

$$\delta^*_\phi = \int_0^\delta \left(1 - \frac{\rho w}{\rho_e w_e}\right)dy$$

With a body fixed coordinate system, the gas dynamic equations for inviscid flow can be written as

$$E_z + F_r + G_\phi + H = 0 \qquad (6)$$

where the flux vectors E, F, G, and H are

$$E = \begin{bmatrix} \rho u \\ \rho u^2+p \\ \rho uv \\ \rho uw \end{bmatrix} \qquad F = \begin{bmatrix} \rho v \\ \rho uv \\ \rho v^2+p \\ \rho vw \end{bmatrix}$$

$$G = \frac{1}{r}\begin{bmatrix} \rho w \\ \rho uw \\ \rho vw \\ \rho w^2+p \end{bmatrix} \qquad H = \frac{1}{r}\begin{bmatrix} \rho v \\ \rho uv \\ \rho(v^2-w^2) \\ 2\rho vw \end{bmatrix}$$

These equations are solved using MacCormack's[6] two-step, predictor-corrector finite difference scheme. The unique feature of the program used here, which was developed by Sanders[7], for the Magnus problem, is that the flow field is computed about an axisymmetric model plus displacement surface. Due to the distortion of the viscous layer caused by interaction of the surface spin, the effective aerodynamic shape has no plane of symmetry.

---

6. *MacCormack, R.W., "The Effect of Viscosity in Hypervelocity Impact Cratering", AIAA Paper No. 69-364, 1969.*

7. *Sanders, B.R. and Dwyer, H.A., "Magnus Forces on Spinning Supersonic Cones. Part II: The Inviscid Flow", AIAA Journal, Vol. 14, May 1976, pp. 576-582.*

The flow field variables resulting from these computation steps have been developed to yield the following aerodynamic coefficients--pitching moment, normal force, center of pressure, Magnus force, Magnus moment, Magnus center of pressure, form drag, viscous drag, and roll damping. The computational time for a single body configuration and flow field condition is approximately ten minutes on a CDC 7600 computer.

C. Coning Motion Computations

In order to compute the effective pitch damping, the technique developed by Schiff[8] is used. This computational technique relates the side moment on a body undergoing a steady coning motion about the CG location to the pitch damping $(C_{M_q} + C_{M_{\dot{\alpha}}})$, see Figure 5.

The numerical technique is MacCormack's[6] predictor-corrector, explicit marching scheme. This computation involves the solution of the Euler equations including terms for Coriolis $[2\rho(\bar{\Omega}\times\bar{v})]$ and centrifugal $[\rho\bar{\Omega}\times(\bar{\Omega}\times\bar{r})]$ forces in a body fixed coordinate system. For this case, the H vector in equation 6 becomes

$$H = \frac{1}{r}\begin{bmatrix} \rho v \\ \rho uv+\rho r[2(\omega_2 w-\omega_3 v)+\omega_1\omega_2 r-z(\omega_2^2+\omega_3^2)] \\ \rho(v^2-w^2)+\rho r[2(\omega_3 u-\omega_1 w)+\omega_1\omega_2 z-r(\omega_1^2+\omega_3^2)] \\ 2\rho vw+\rho r[2(\omega_1 v-\omega_2 u)+\omega_3(\omega_2 r+\omega_1 z)] \end{bmatrix}$$

where ω_1, ω_2, and ω_3 are the components of the angular velocity vector $(\dot{\theta})$ resolved in the z, r, and ϕ directions, respectively.

For the case of a steady coning motion, the flow field is time-invariant in the body-fixed coordinate system. The effective pitch damping $(C_{M_q} + C_{M_{\dot{\alpha}}})$ is determined using the relation

$$C_{n_{\dot{\theta}}} \approx \sin\sigma(C_{M_q} + C_{M_{\dot{\alpha}}}) \qquad (7)$$

where $C_{n_{\dot{\theta}}}$ = side moment at coning rate $\dot{\theta}$ and effective angle of attack σ, which is valid for small values of σ and $\dot{\theta}$. Thus a dynamic aerodynamic parameter is determined using a steady flow field computation. This is a potentially very useful tool for the exterior ballistician. The computation time is approximately 90 seconds on a CDC 7600 computer for the body configurations in this study.

---

8. *Schiff, L.B., "Nonlinear Aerodynamics of Bodies of Coning Motion", AIAA Journal, Vol. 10, No. 11, November 1972, pp. 1517-1522.*

III. RESULTS

A. Comparisons to Experiment

Detailed comparisons of the computations to experimental data for turbulent boundary layer profile characteristics, wall pressure measurements and Magnus force are reported in Ref. 9. Comparisons shown here will be limited to the aerodynamic coefficients of interest.

Charters and Kent[10] have shown that roll damping can be related to the skin friction drag for a cylinder according to the relation

$$C_{\ell p} = -0.25\ C_{DBL} \tag{8}$$

Murphy[11] has shown good agreement with this relation in a series of free flight range tests firings of two caliber tangent ogive cylinder models with total lengths of 5, 7, and 9 calibers.

The results of this computational study confirm that equation (8) is a good engineering relation for estimating the roll damping coefficient. A summary of the computed results are compared to the Charters-Kent relation in Figure 6. The computational results show a spread which is due to the effect of ogive configuration. This effect is better illustrated in Figure 7 where roll damping is plotted versus projectile length for four ogive configurations at Mach 2.75. In general, this computational study shows that roll damping is linear with respect to body length for a particular flight velocity and that the zero offset is a function of ogive configuration.

Examples of comparisons of the computed results to experimental data are presented in Figures 8 through 12. The comparisons for pitch plane static parameters shown in Figures 8, 9 and 10 indicate excellent agreement for $M > 2.5$. The results for the supersonic marching computational technique used here have indicated a reduced accuracy for flow over shell with short ogives at low supersonic velocities. The limited comparison for Magnus in Figure 11

---

9. *Sturek, W.B., Dwyer, H. A., Kayser, L. D., Nietubicz, C. J., Reklis, R. P. and Opalka, K. O., "Computations of Magnus Effects for a Yawed, Spinning Body of Revolution", AIAA Journal, Vol. 16, No. 7, July 1978, pp. 687-692.*

10. *Charters, A.C. and Kent, R.H., "The Relation Between the Skin Friction Drag and the Spin Reducing Torque", BRL Report No. 287, US Army Ballistic Research Laboratory/ARRADCOM, Aberdeen Proving Ground, Maryland 21005, 1942. AD 491854.*

11. *Murphy, C.H. and Schmidt, L.E., "The Effect of Length on the Aerodyramic Characteristics of Bodies of Revolution in Supersonic Flight", BRL Report No. 876, US Army Ballistic Research Laboratory/ARRADCOM, Aberdeen Proving Ground, Maryland 21005, August 1973. AD 23468.*

indicates acceptable agreement if allowance is made for the small magnitude of the Magnus effect and the variance between the wind tunnel and range experimental measurements. A comparson between computation and experiment for pitch damping is shown in Figure 12. The experimental point, which is for an L/D of 5.12 and cone angle of 9.52°, shows excellent agreement with the trend of the computed results. A similar comparison for pitch damping is shown in Figure 13 for a 10° cone. This comparison includes both wind tunnel and free flight range data. The pitch damping is very small for a cone; but the agreement shown is considered to be very good. In general, it is felt that the numerical computations do provide an accuracy for the aerodynamic coefficients that is within the uncertainty of our ability to determine these coefficients experimentally. However, it is felt that a broader scope of comparison for the aerodynamic coefficients between experiment and computation is of interest and increased effort to accomplish this is underway.

B. Parametric Comparisons

Examples illustrating the parametric results are shown in Figures 14 through 30. The series of comparisons shown in Figures 14 through 23 illustrates an example for each aerodynamic coefficient computed in this study. The case chosen is the SOC model for a total length of six calibers and for ogive lengths of two, three, and four calibers. The aerodynamic coefficients are plotted versus Mach number for atmospheric free stream launch conditions assuming an adiabatic wall temperature boundary condition. These comparisons show, for a fixed body length, that configurations with long slender ogives have reduced pitch damping, less drag, and a reduced Magnus moment compared to bodies with shorter ogive lengths. The development of the Magnus force over the full length of the shell is shown in Figure 24 for two ogive configurations and a total length of six calibers. This figure shows that the Magnus effect is strongly dependent on the length of the cylindrical afterbody. Only a small portion of the Magnus force is generated on the ogive. Examples are shown in Figures 25 through 27 illustrating the effects of variations in ogive shape for fixed forebody and total projectile lengths. These comparisons show that pitching moment, Magnus moment, and pitch damping are increased as ogive bluntness is increased. The final sequence of parametric comparisons is shown in Figures 28 through 30 where the effect of varying the body length is shown for a fixed ogive shape. These figures show that pitching moment, Magnus moment, and pitch damping are all increased as the body length is increased.

The comparisons shown represent a small fraction of the potential comparisons possible from the total data base generated. The intent here has been to illustrate the capability of the computation techniques rather than develop any conclusion as to the relative superiority of any particular configuration. This study is part of a continuing effort that is being expanded to include boattail configurations and a wider Mach number range--transonic velocities are of particular interest.

IV. SUMMARY

A computational aerodynamics parametric study has been described in which advanced numerical techniques for computing three-dimensional inviscid and turbulent viscous supersonic flow fields have been used. A comprehensive data

base has been generated for cone-cylinder, tangent-ogive-cylinder, and secant-ogive-cylinder configurations. Of particular interest are the computations of Magnus effects, which are accomplished in a conceptually exact manner, and the computations of pitch damping. Comparisons between the computed results and experiment have provided verification of the computational techniques. Comparisons of the computed results for differing body configurations have established the ability of the computational techniques to distinguish the effects of body configuration on the aerodynamic coefficients.

REFERENCES

1. Whyte, R., "SPIN-73, An Updated Version of the Spinner Computer Program," Picatinny Arsenal Technical Report 4588, November 1973.

2. Moore, F.G. and McKerley, C.W., "Aerodynamics of Guided and Unguided Weapons; Part II-Computer Program and Usage", NWL TR-3036, 1974.

3. Moore, F.G. and Swanson, R.C., "Aerodynamics of Tactical Weapons to Mach Number 3 and Angle of Attack 15°, Part I- Theory and Application", NSWC/DL TR-3584, February 1977.

4. Dwyer, H.A. and Sanders, B.R., "Magnus Forces on Spinning Supersonic Cones. Part I: The Boundary Layer", AIAA Journal, Vol. 14, April 1976, pp. 498-504.

5. Moore, F.N., "Displacement Effect of a Three-Dimensional Boundary Layer", NACA TN 2722. June 1952.

6. MacCormack, R.W., "The Effect of Viscosity in Hypervelocity Impact Cratering", AIAA Paper No. 69-364, 1969.

7. Sanders, B.R. and Dwyer, H.A., "Magnus Forces on Spinning Supersonic Cones. Part II: The Inviscid Flow", AIAA Journal, Vol. 14, May 1976, pp. 576-582.

8. Schiff, L.B., "Nonlinear Aerodynamics of Bodies of Coning Motion", AIAA Journal, Vol. 10, No. 11, November 1972, pp. 1517-1522.

9. Sturek, W.B., Dwyer, H. A., Kayser, L. D., Nietubicz, C. J., Reklis, R. P. and Opalka, K. O., "Computations of Magnus Effects for a Yawed, Spinning Body of Revolution", AIAA Journal, Vol. 16, No. 7, July 1978, pp. 687-692.

10. Charters, A.C. and Kent, R.H., "The Relation Between the Skin Friction Drag and the Spin Reducing Torque", BRL Report No. 287, US Army Ballistic Research Laboratory/ARRADCOM, Aberdeen Proving Ground, Maryland 21005, 1942. AD 491854.

11. Murphy, C.H. and Schmidt, L.E., "The Effect of Length on the Aerodynamic Characteristics of Bodies of Revolution in Supersonic Flight", BRL Report No. 876, US Army Ballistic Research Laboratory/ARRADCOM, Aberdeen Proving Ground, Maryland 21005, August 1973. AD 23468.

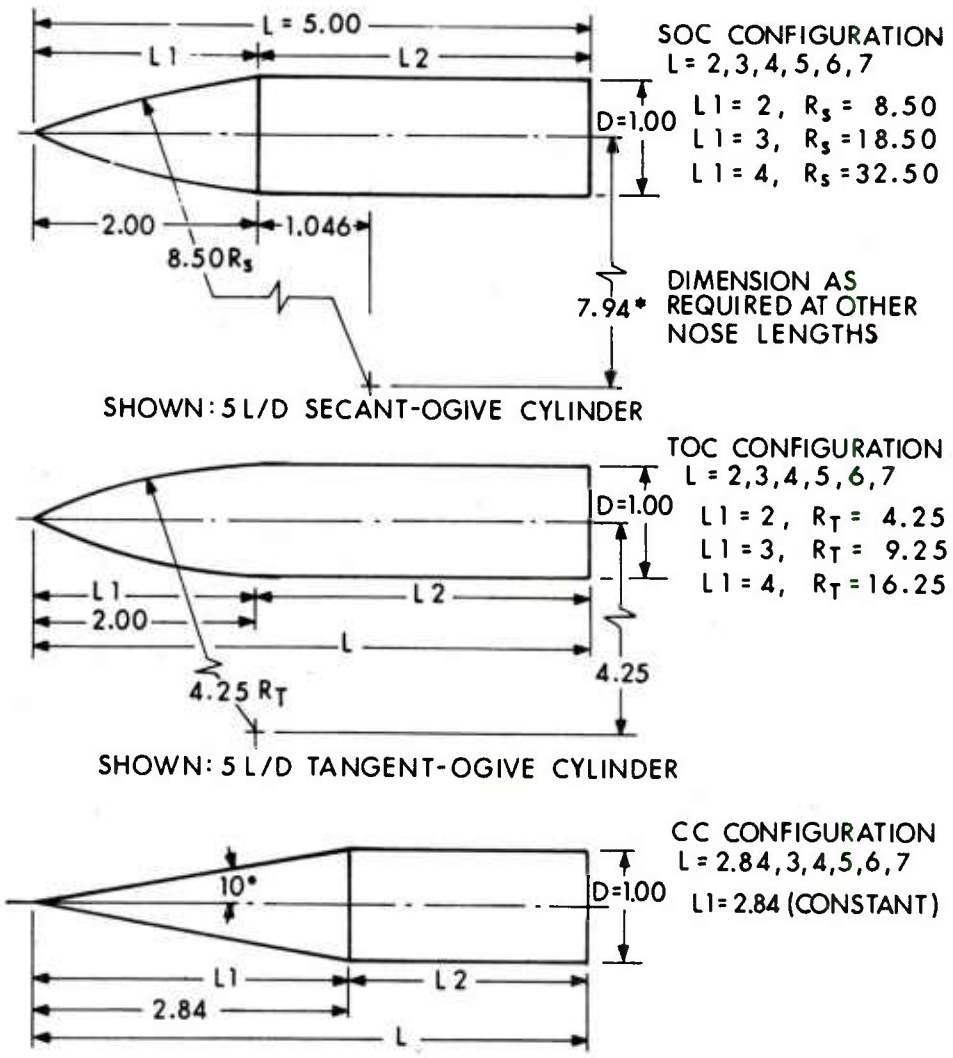

Figure 1. Model Geometries

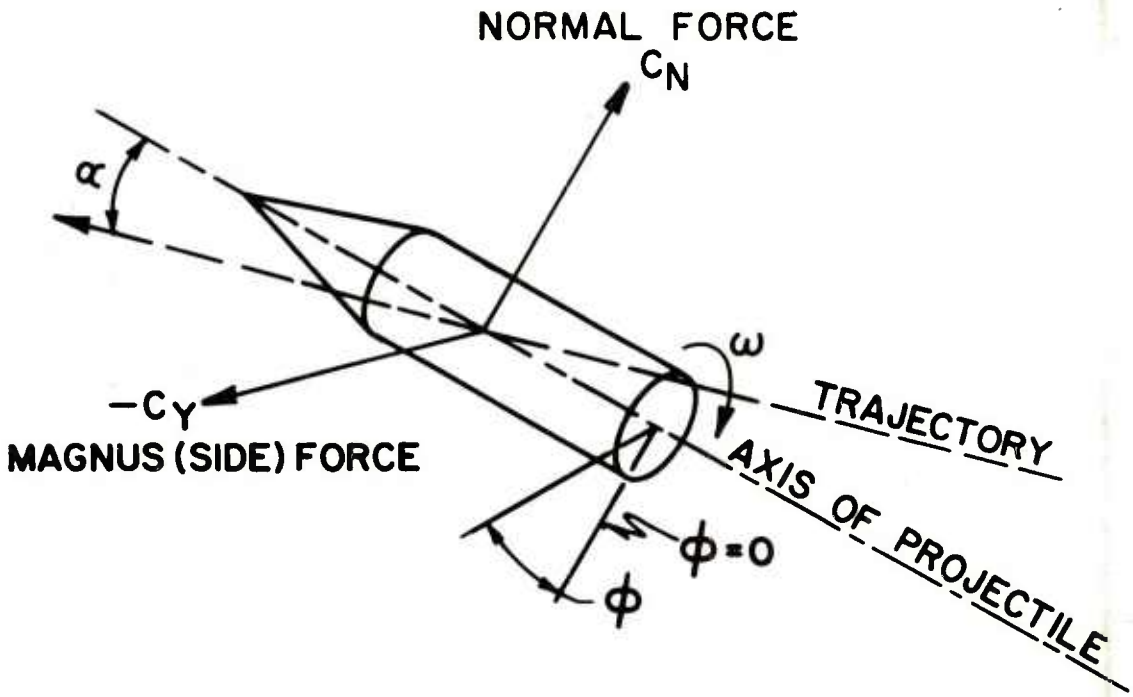

Figure 2. Magnus and Normal Forces on Spinning Projectile

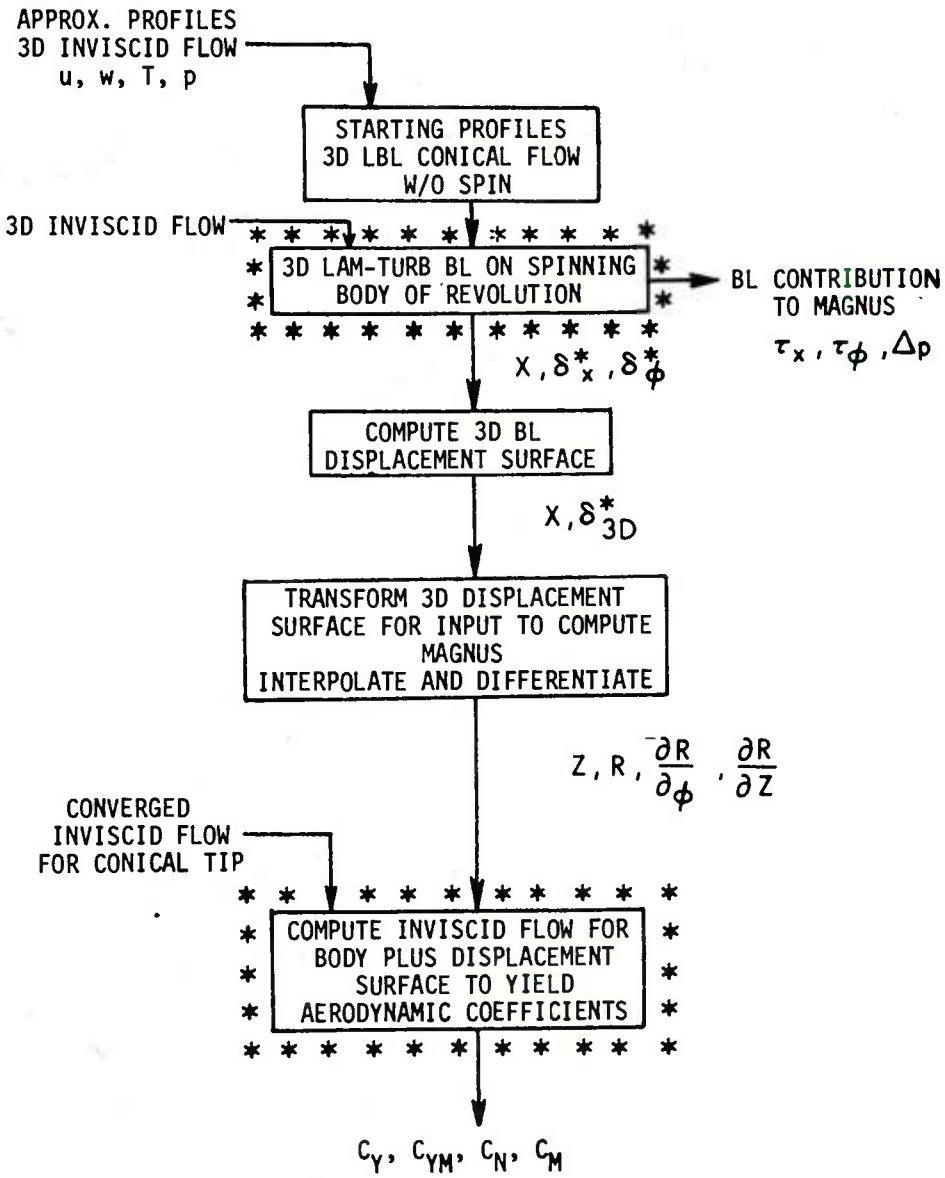

Figure 3. Sequence of Computations

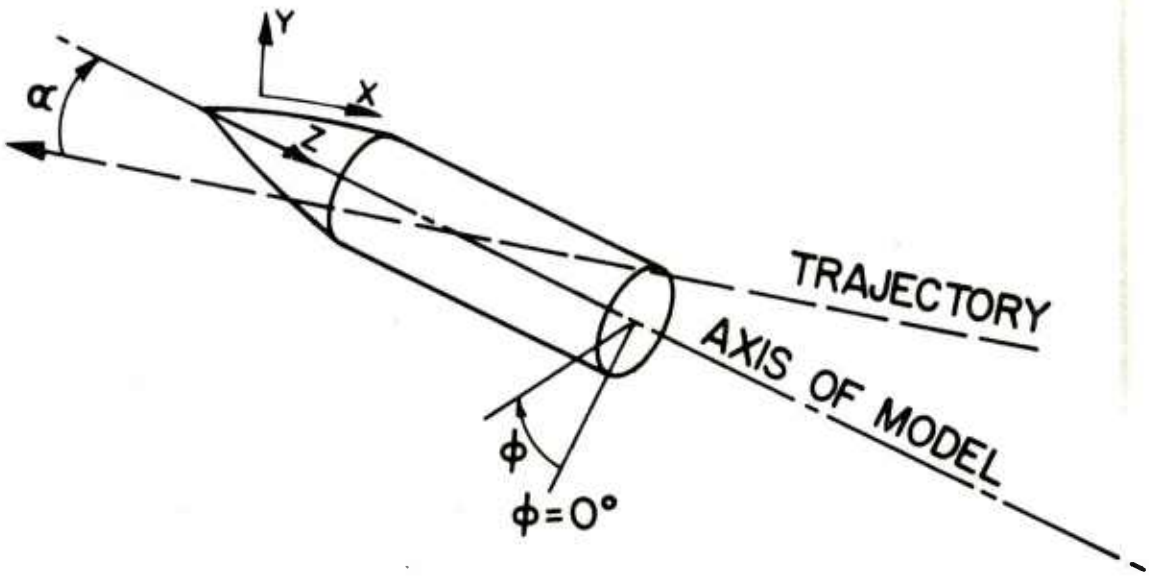

Figure 4. Coordinate System

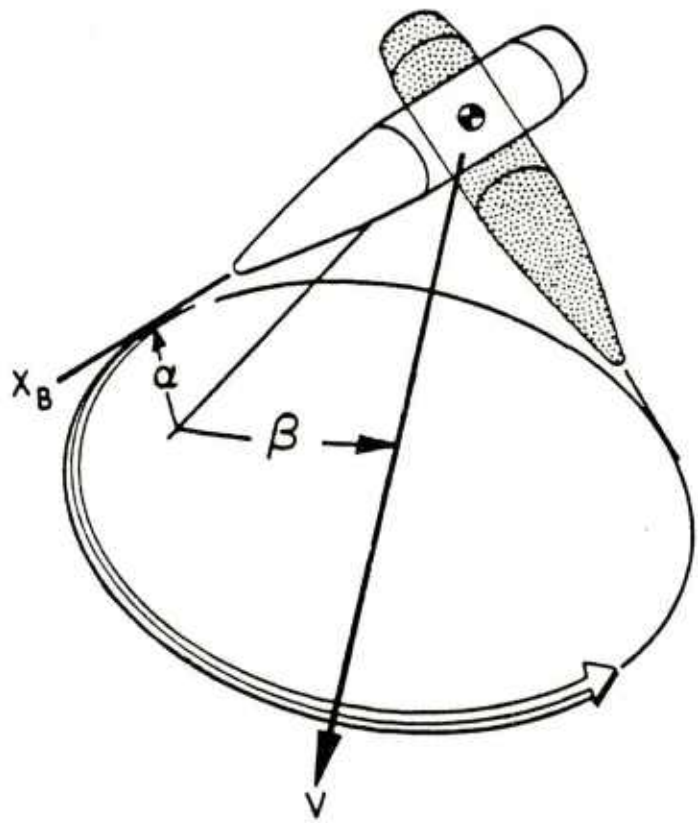

Figure 5. Coning Motion About Center of Gravity

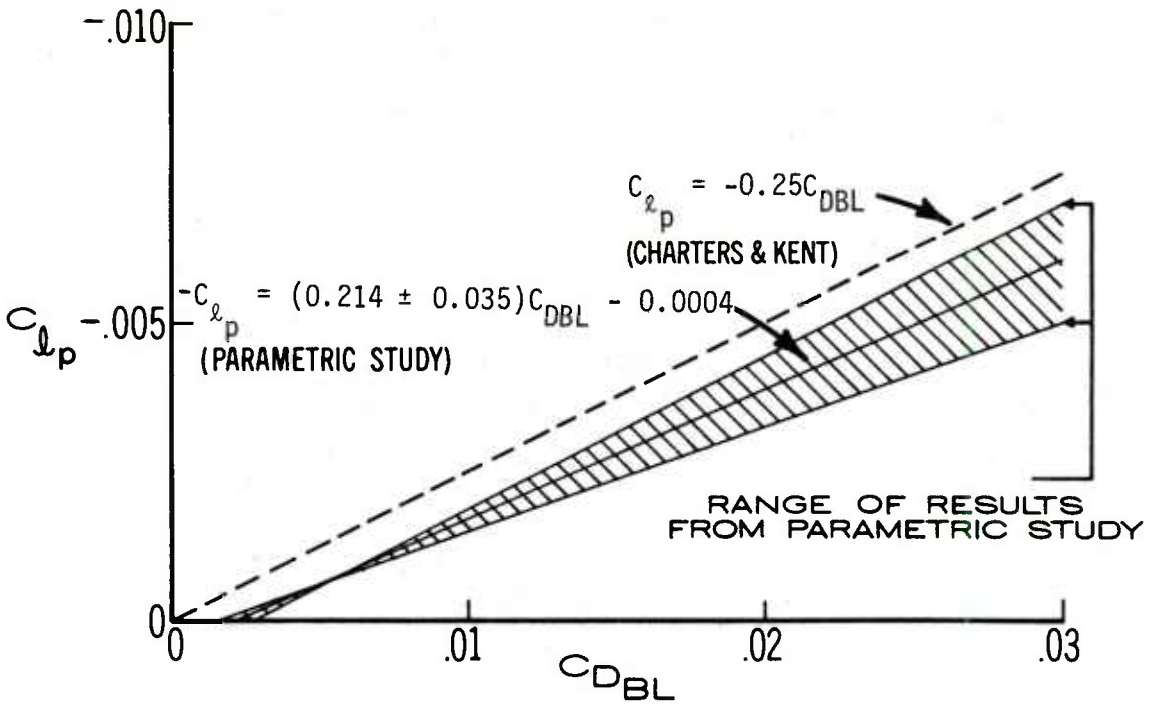

Figure 6. Comparison of Parametric Roll Damping Computations to the Charters and Kent Relation

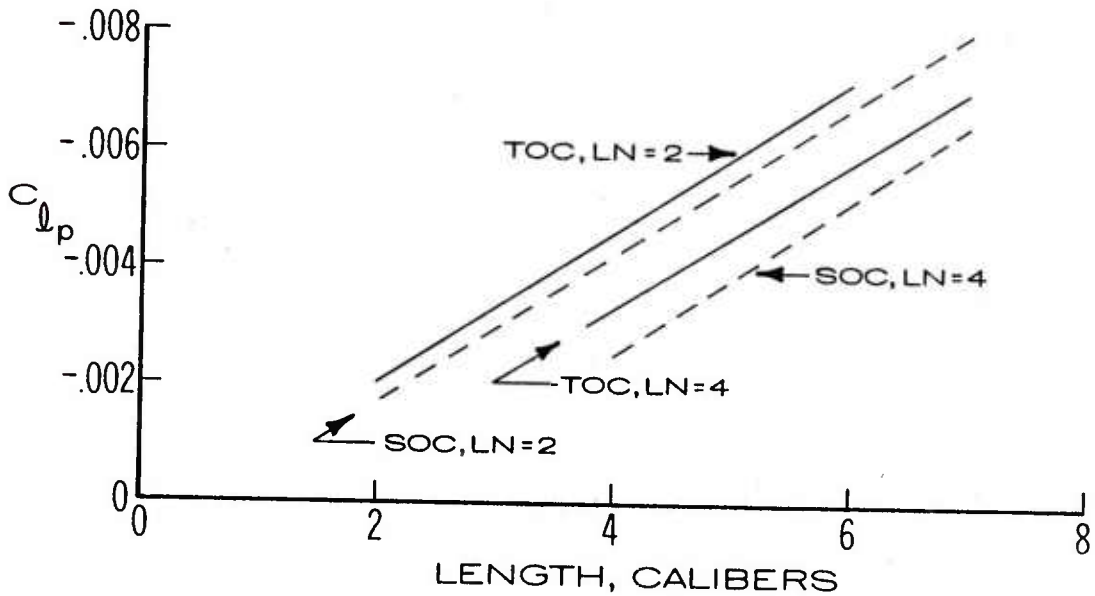

Figure 7. Roll Damping Versus Projectile Length at M = 2.75

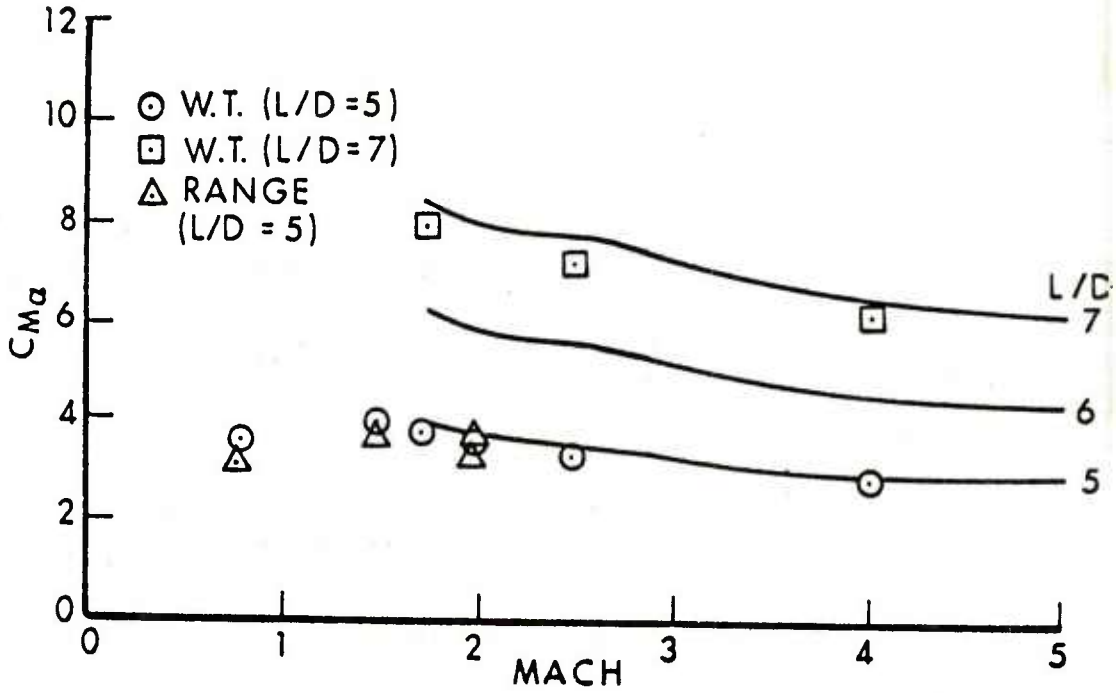

Figure 8. Pitching Moment, Comparison with Experiment, SOC Model, LN = 2, C.G. at 0.6L Behind Nose

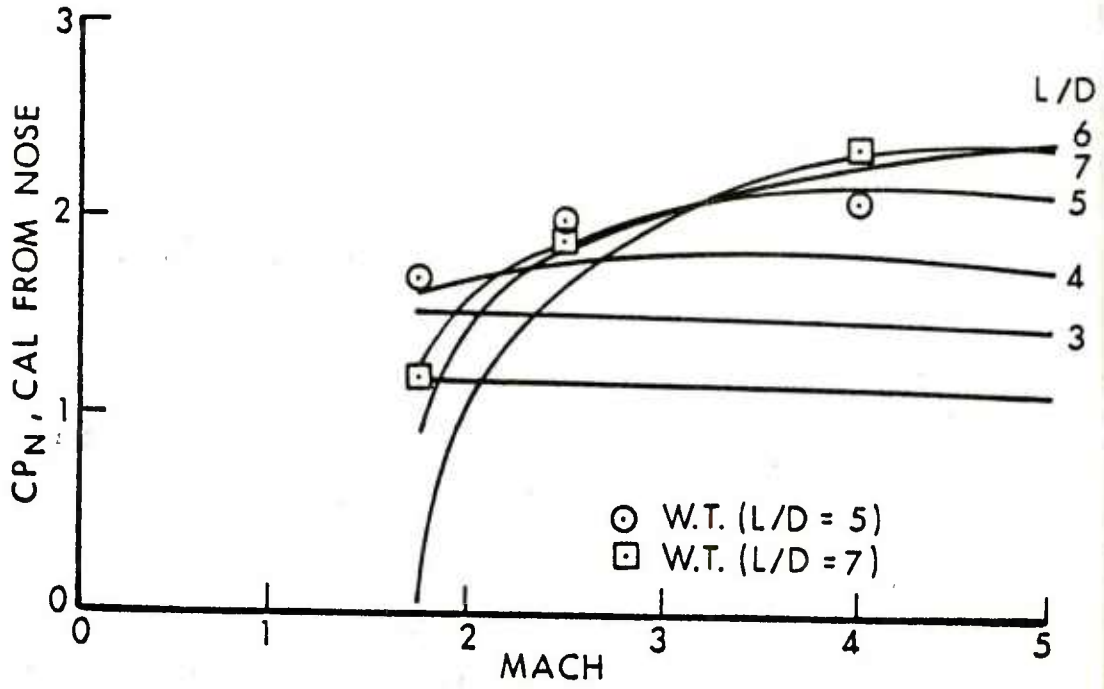

Figure 9. Center of Pressure, Comparison with Experiment, SOC Model, LN = 2

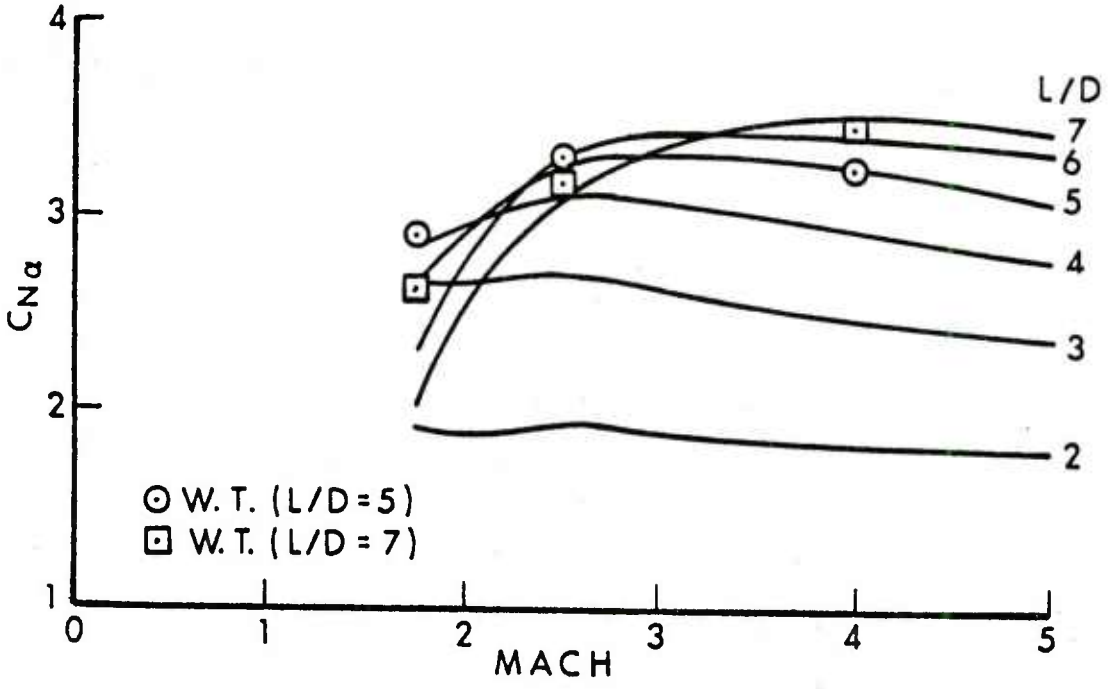

Figure 10. Normal Force, Comparison with Experiment, SOC Model, LN = 2

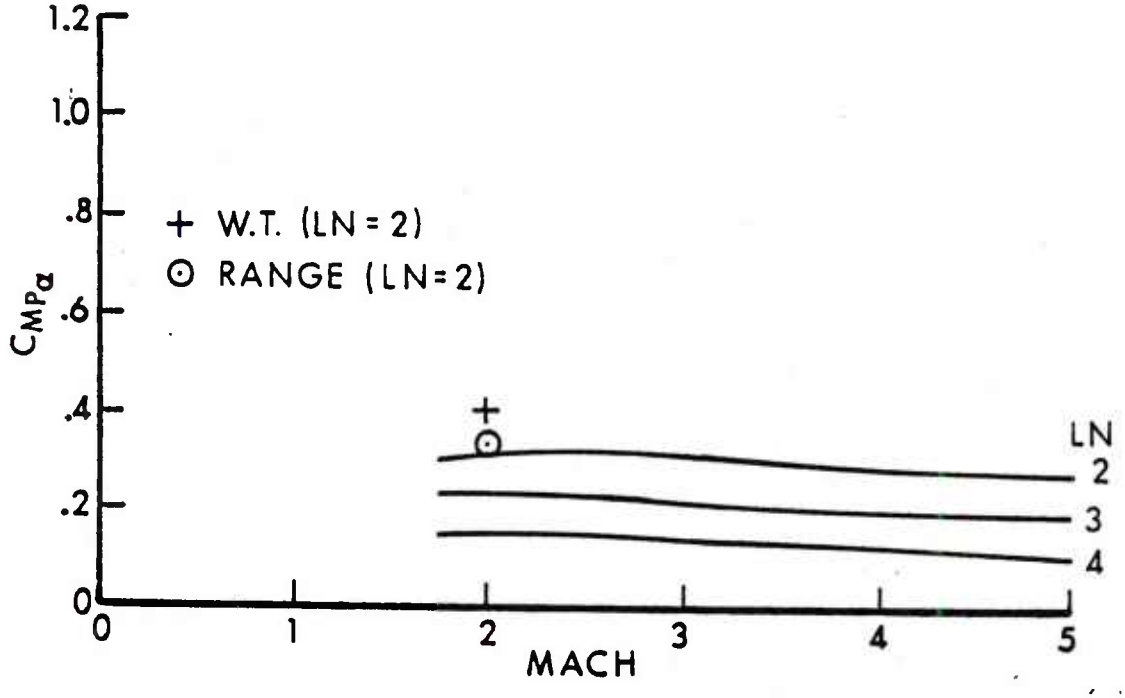

Figure 11. Magnus Moment, Comparison with Experiment, SOC Model, L/D = 5, C.G. at 0.6L Behind Nose

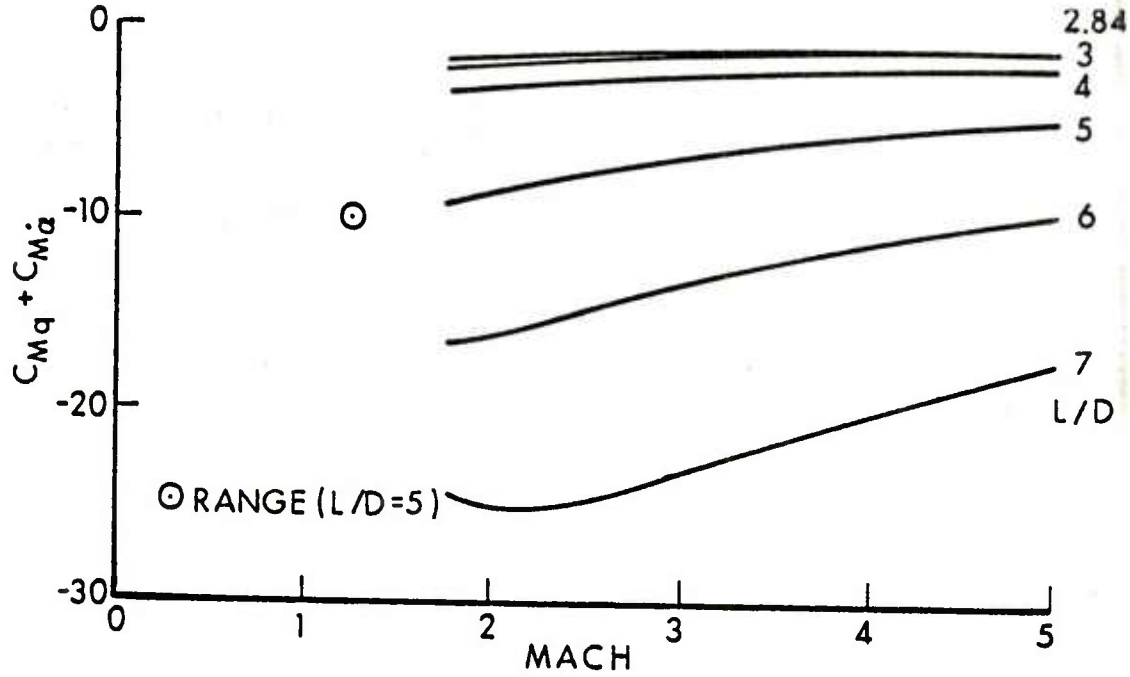

Figure 12. Pitch Damping, Comparison with Experiment, Cone-Cylinder Model, C.G. at 0.6L Behind Nose

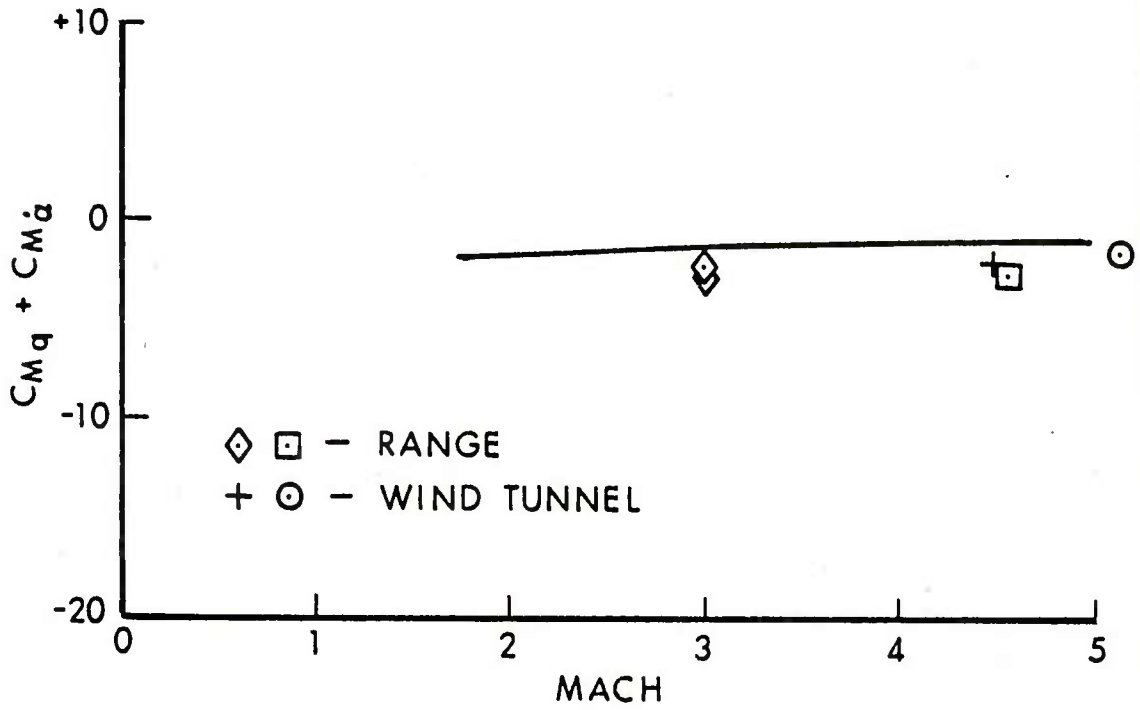

Figure 13. Pitch Damping, Comparison with Experiment, 10° Cone Model, C.G. at 0.6L Behind Nose

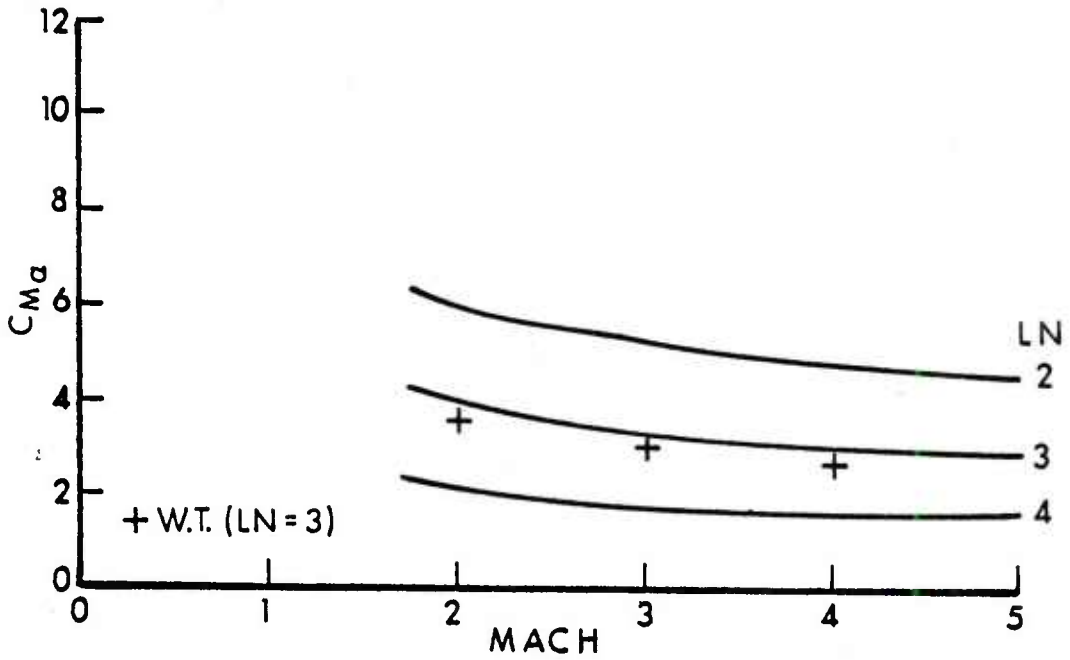

Figure 14. Pitching Moment, Parametric Comparison, SOC, L/D = 6, C.G. at 0.6L Behind Nose

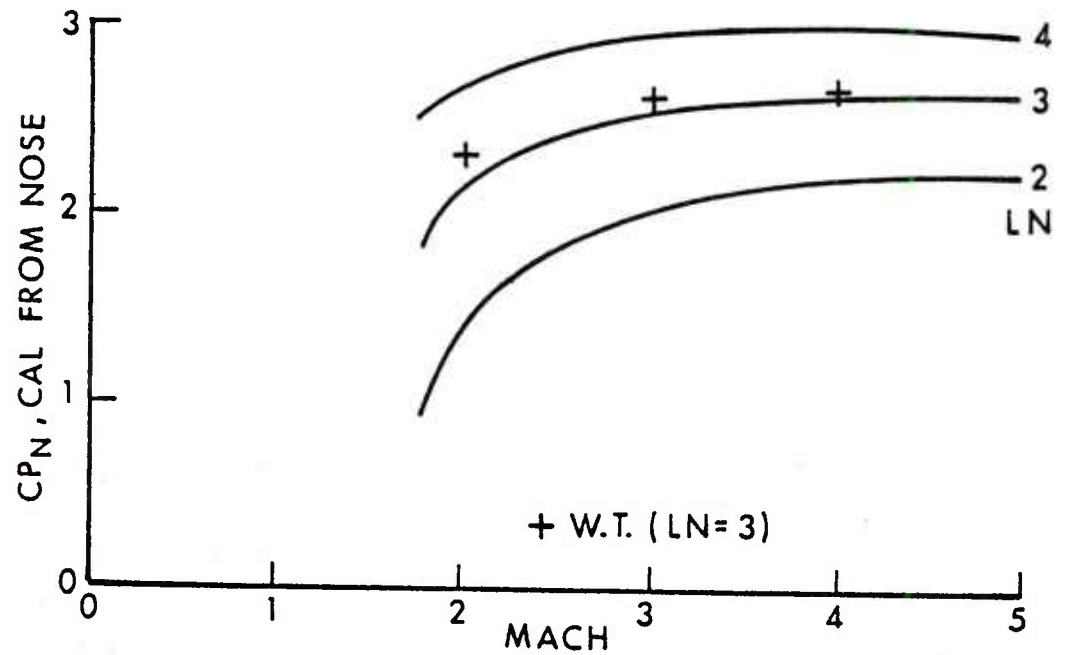

Figure 15. Center of Pressure, Parametric Comparison, SOC, L/D = 6

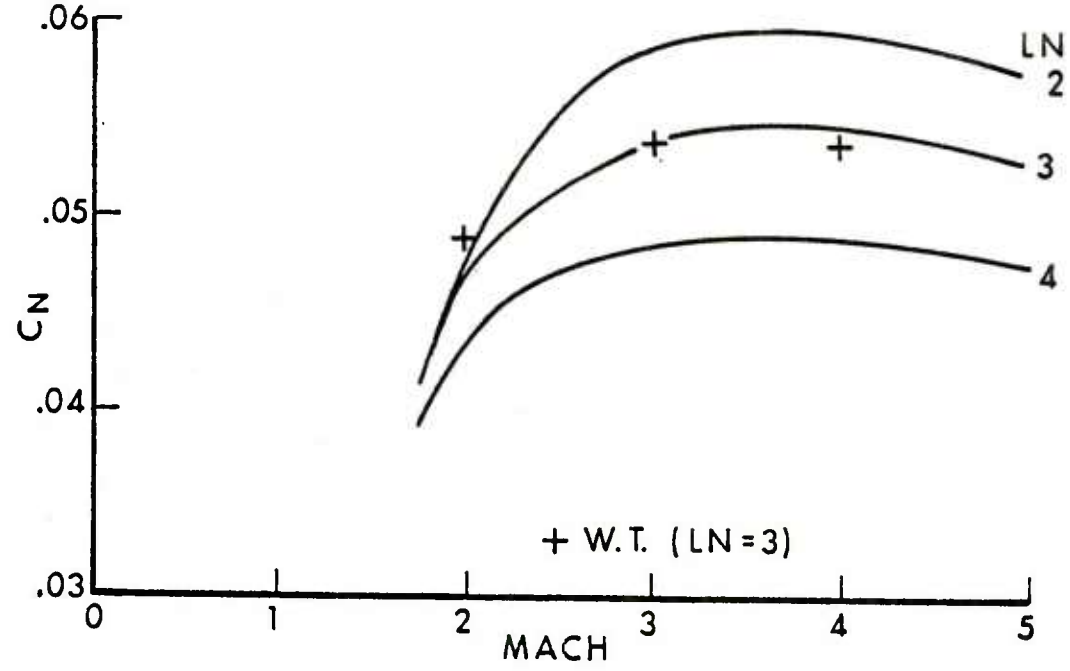

Figure 16. Normal Force, Parametric Comparison, SOC, L/D = 6, α = 1°

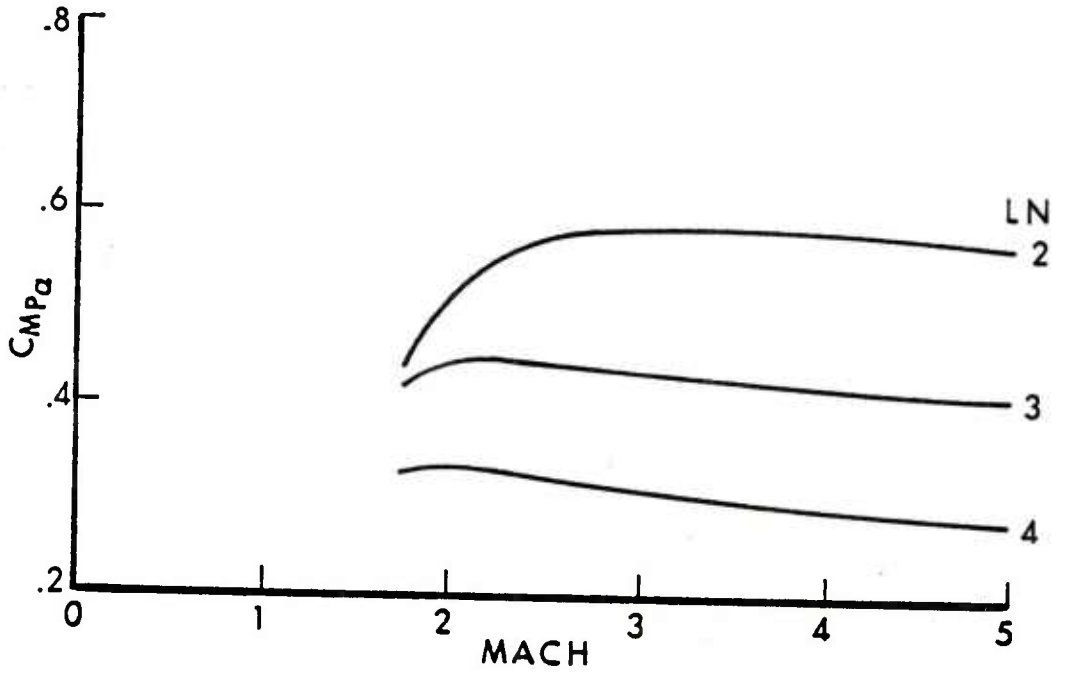

Figure 17. Magnus Moment, Parametric Comparison, SOC, L/D = 6, C.G. at 0.6L Behind Nose

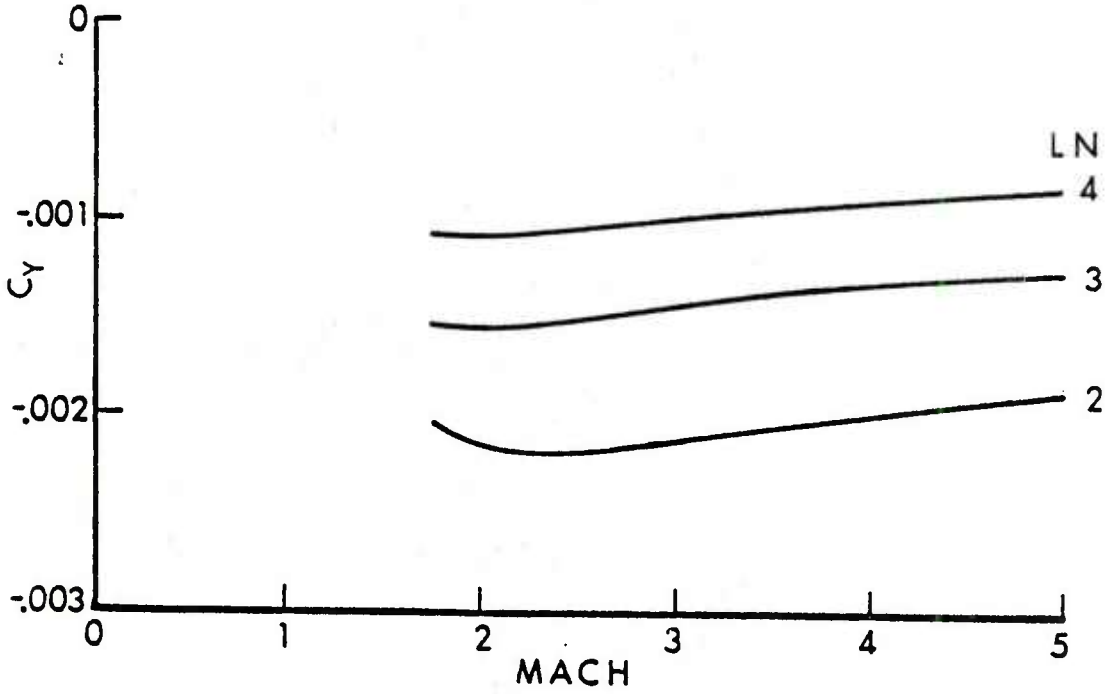

Figure 18. Magnus Force, Parametric Comparison, SOC, L/D = 6, α = 1°, PD/V = 0.19

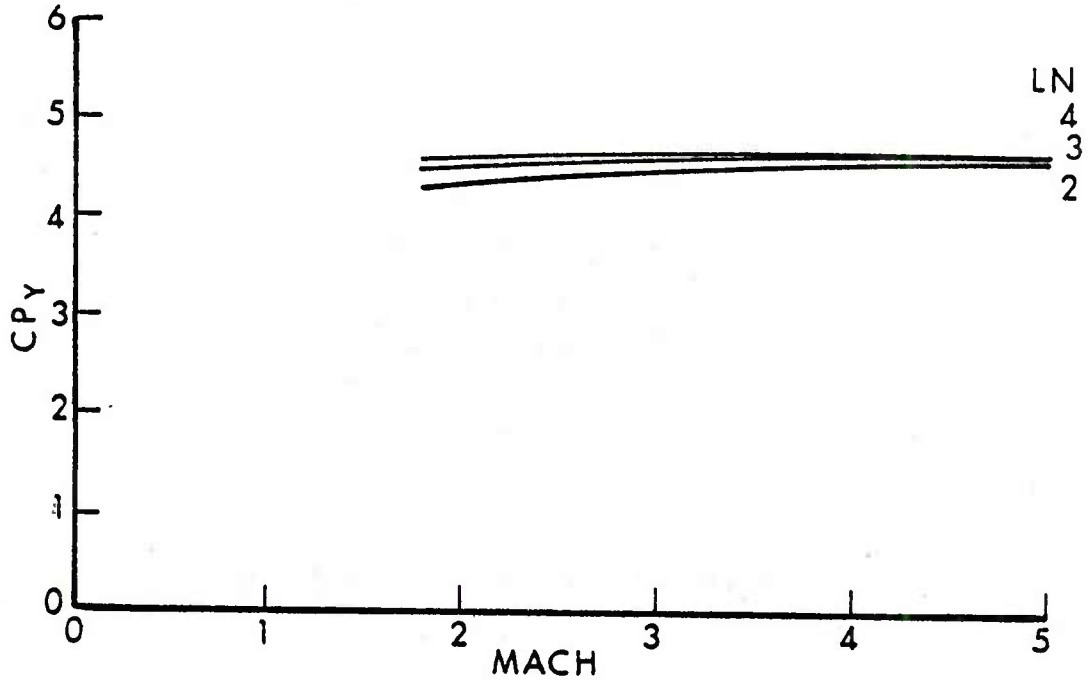

Figure 19. Magnus Center of Pressure, Parametric Comparison, SOC, L/D = 6, α = 1°, PD/V = 0.19

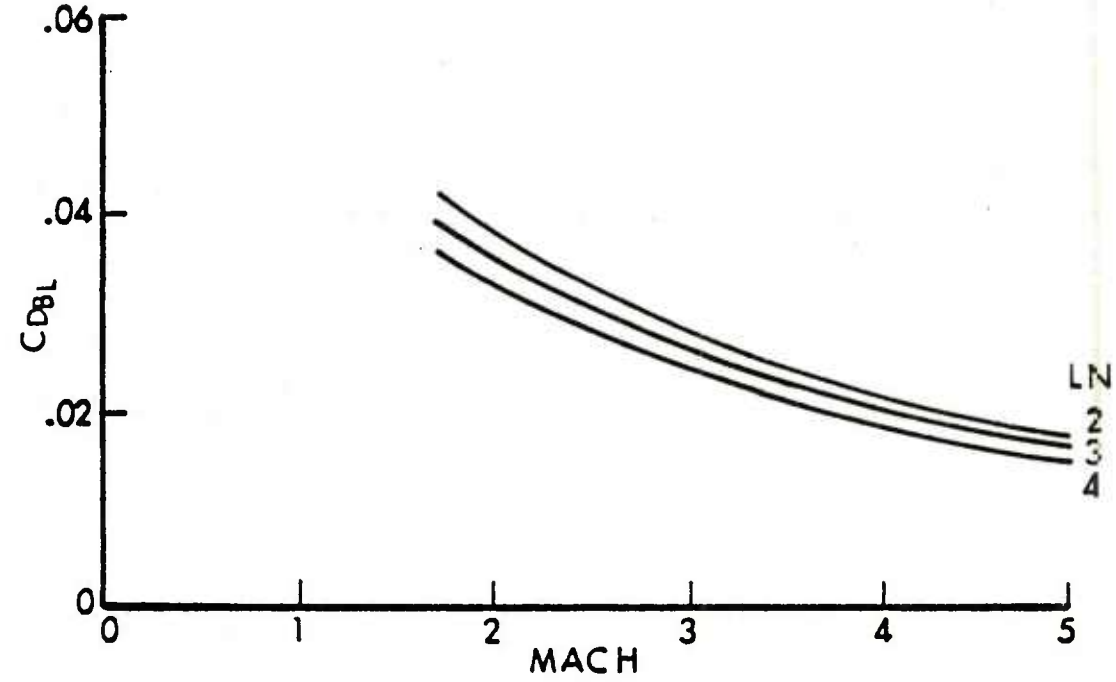

Figure 20. Viscous Drag, Parametric Comparison, SOC, L/D = 6

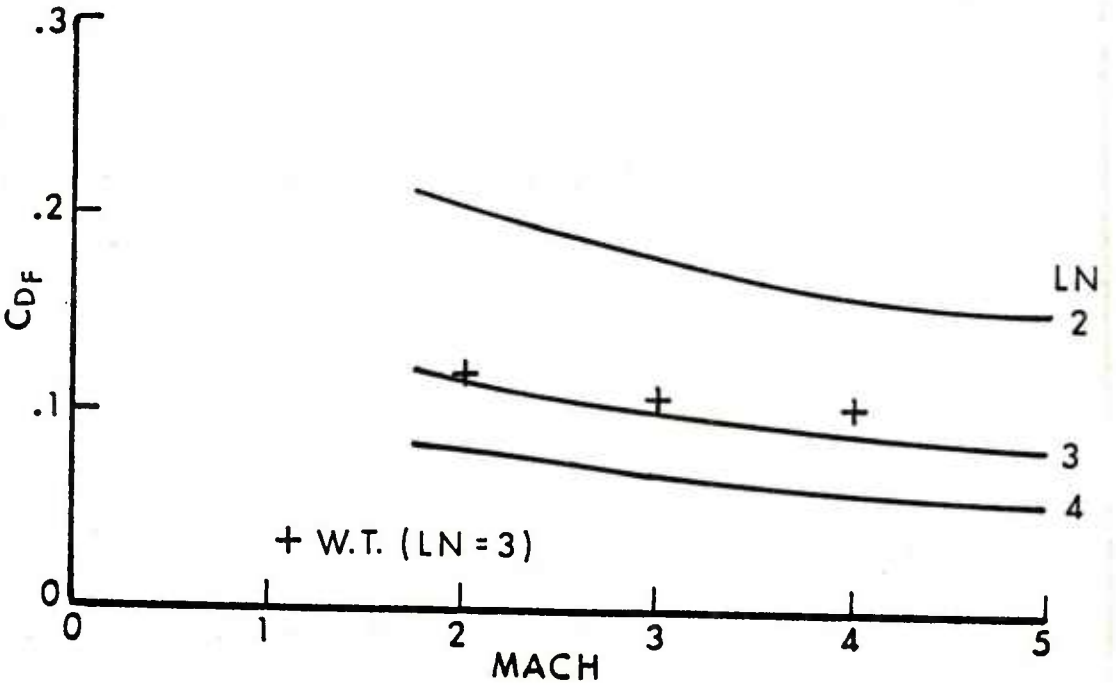

Figure 21. Form Drag Plus Viscous Drag, Parametric Comparison, SOC, L/D = 6

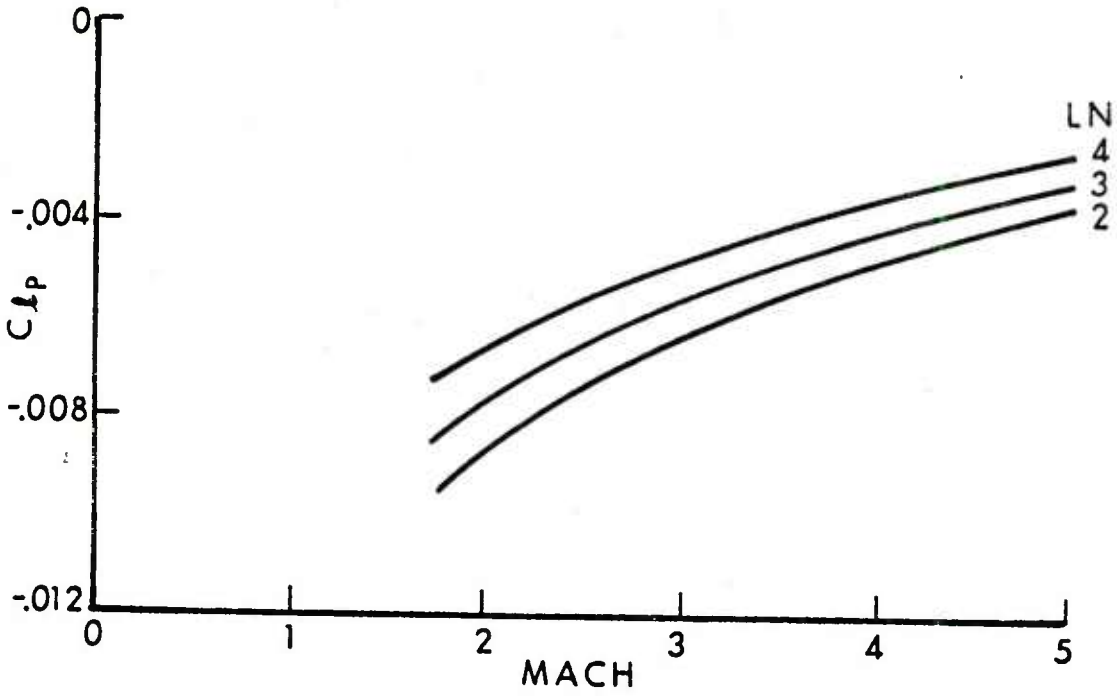

Figure 22. Roll Damping, Parametric Comparison, SOC, L/D = 6

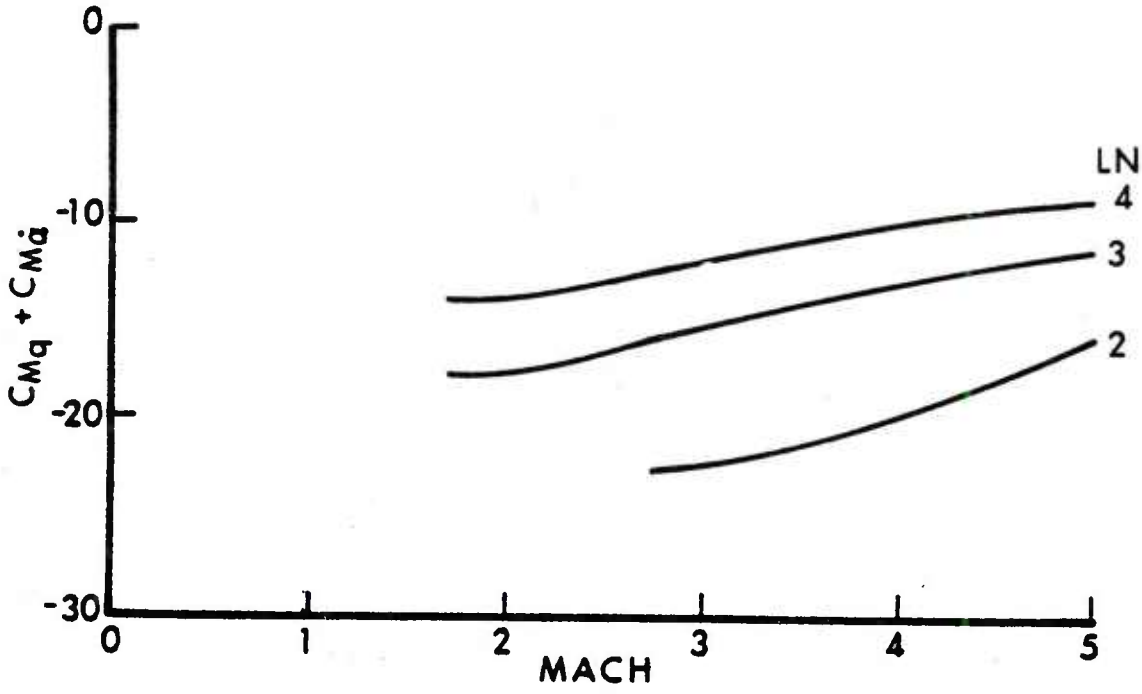

Figure 23. Pitch Damping, Parametric Comparison, SOC, L/D = 6, C.G. at 0.6L Behind Nose

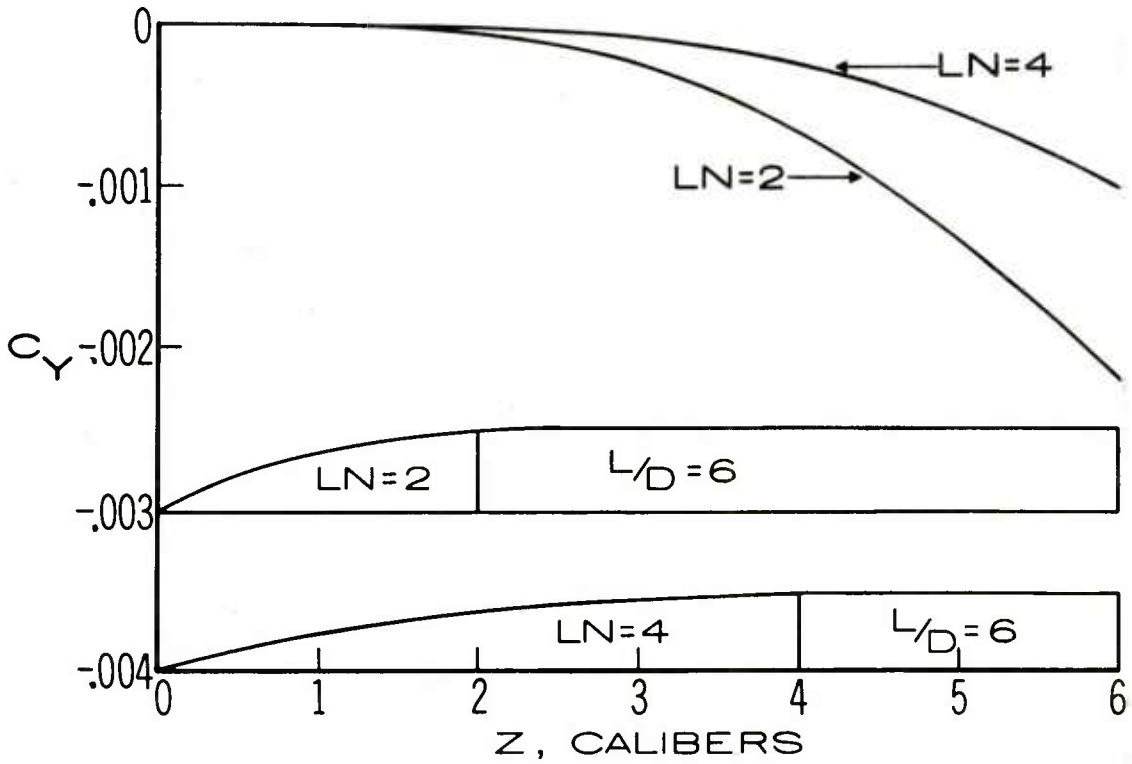

Figure 24. Development of Magnus Force Versus Axial Position, SOC Model, M = 2.75, α = 1°, PD/V = 0.19

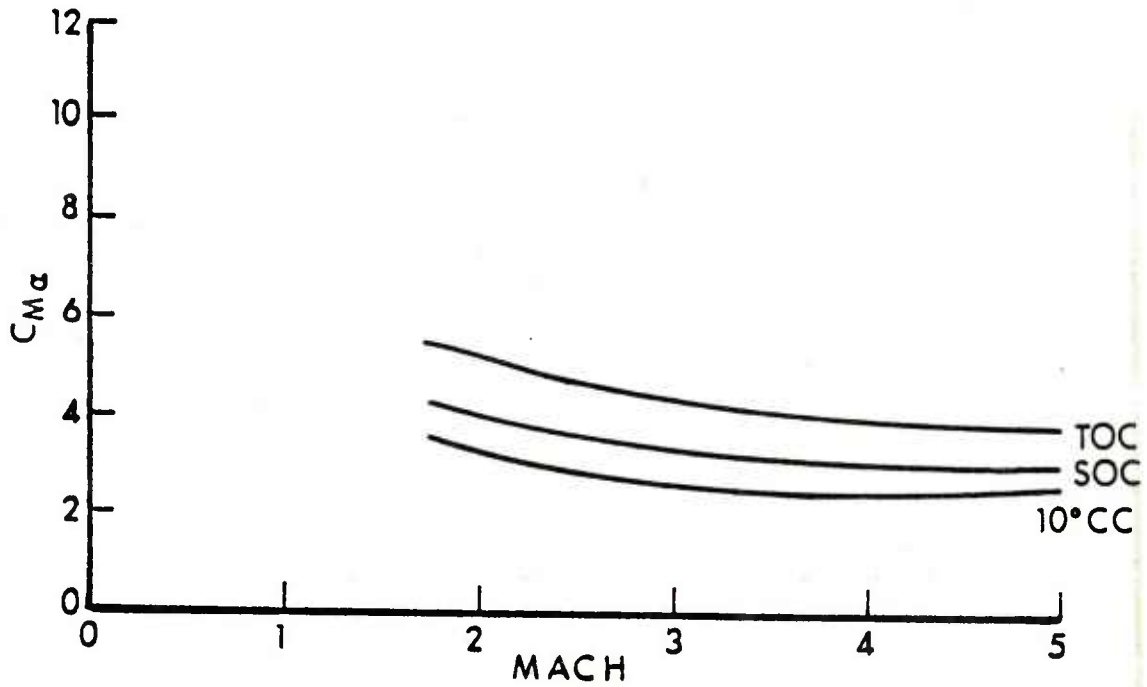

Figure 25. Pitching Moment, Parametric Comparison, L/D = 6, LN = 3, C.G. at 0.6L Behind Nose

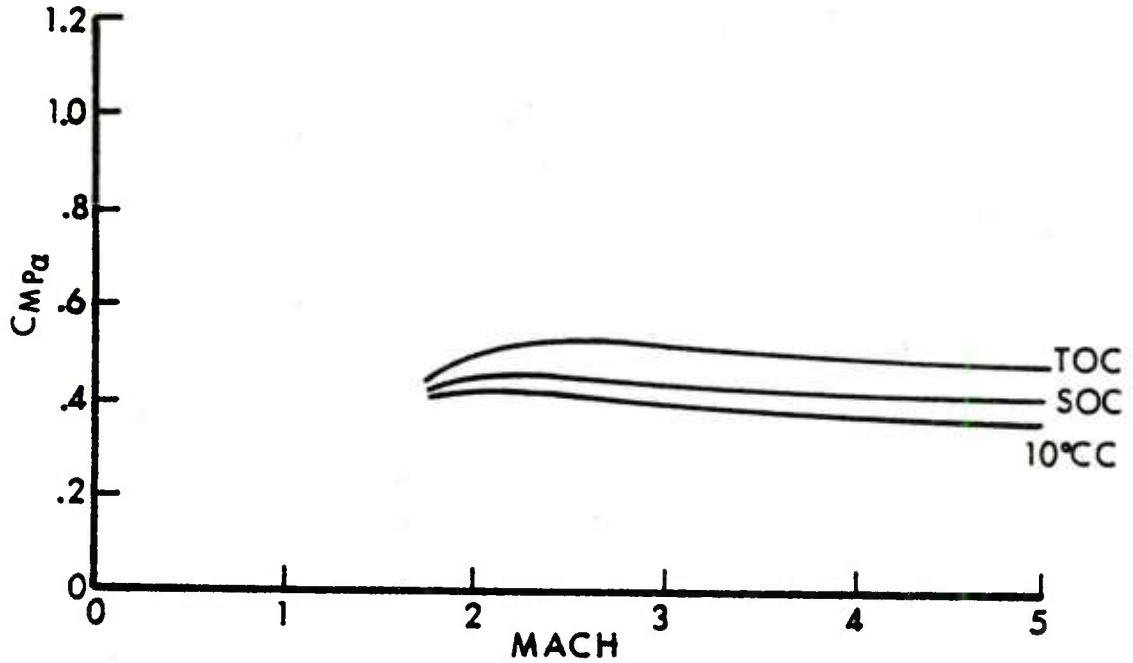

Figure 26. Magnus Moment, Parametric Comparison, L/D = 6, LN = 3, C.G. at 0.6L Behind Nose

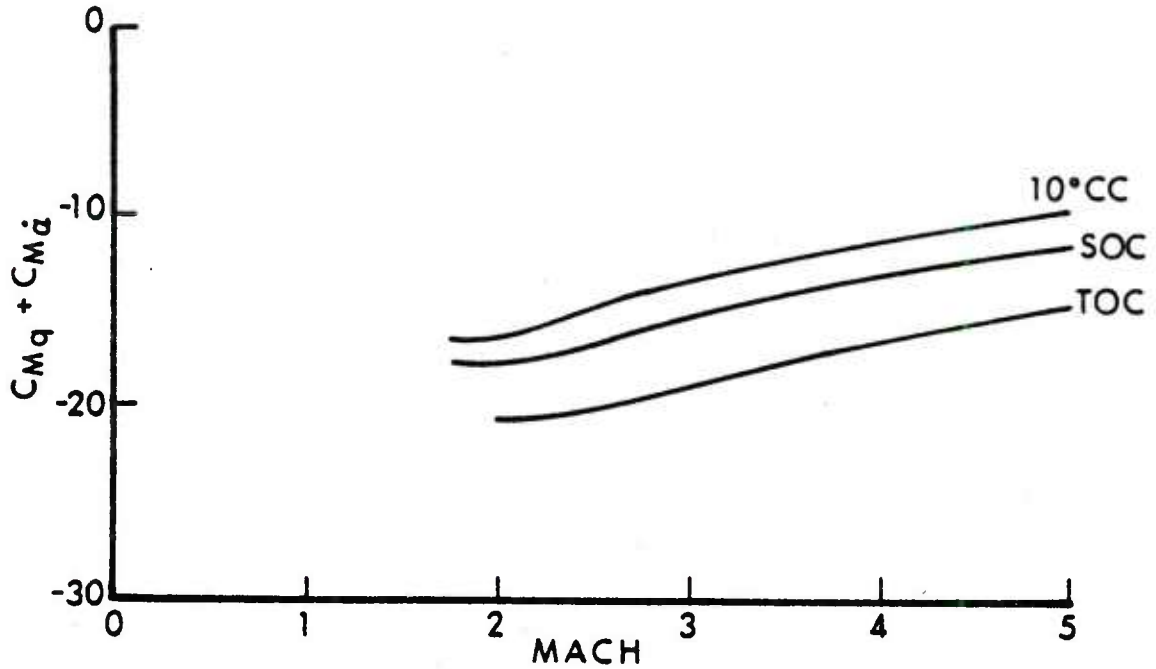

Figure 27. Pitch Damping, Parametric Comparison, L/D = 6, LN = 3, C.G. at 0.6L Behind Nose

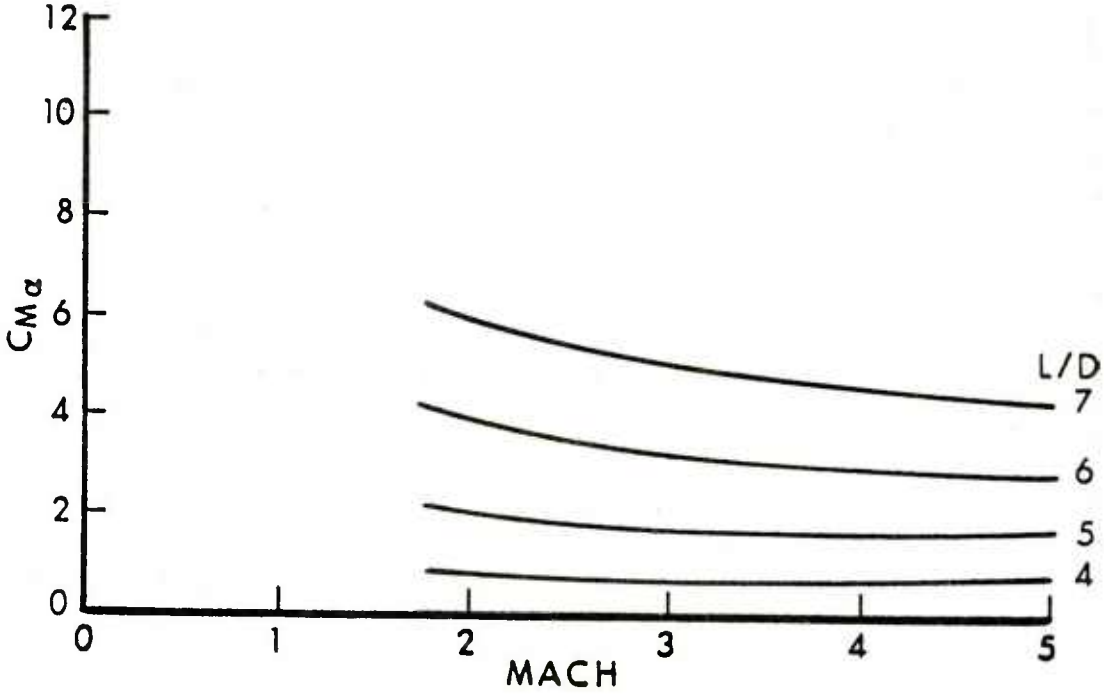

Figure 28. Pitching Moment, Parametric Comparison, SOC, LN = 3, C.G. at 0.6L Behind Nose

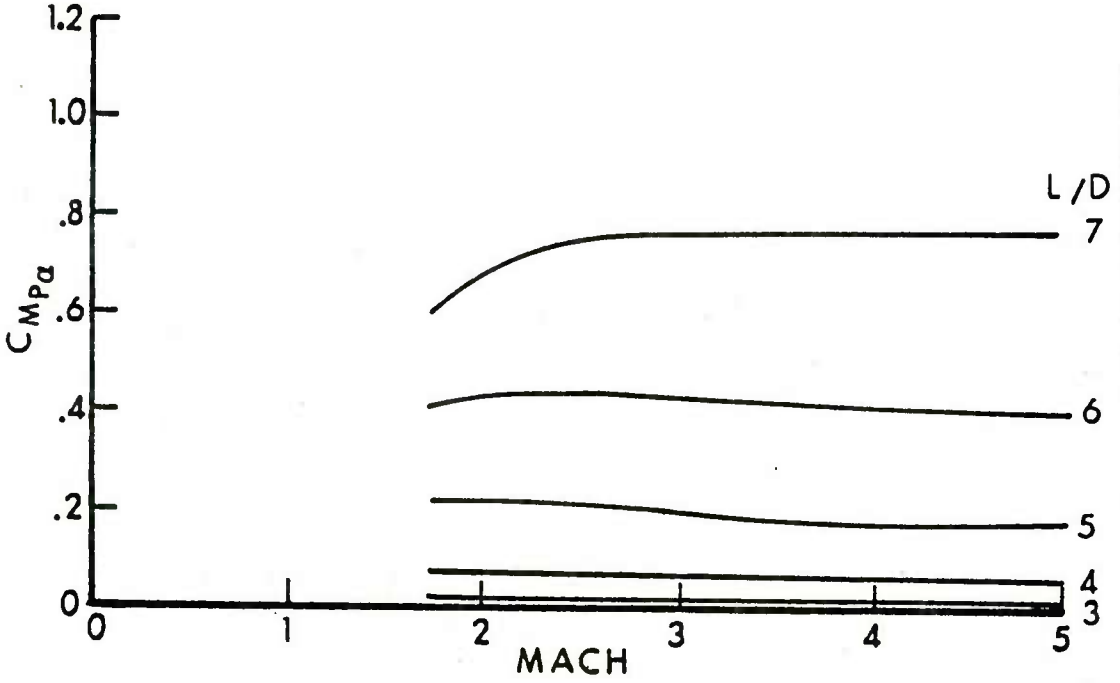

Figure 29. Magnus Moment, Parametric Comparison, SOC, LN = 3, C.G. at 0.6L Behind Nose

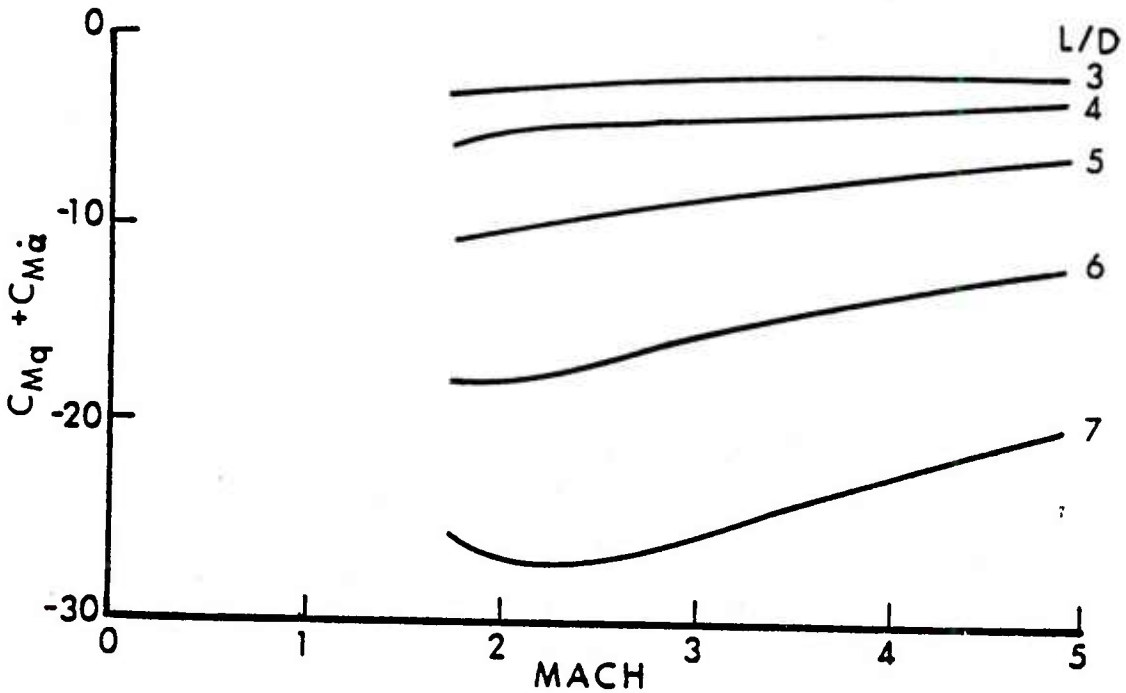

Figure 30. Pitch Damping, Parametric Comparison, SOC, LN = 3, C.G. at 0.6L Behind Nose

LIST OF SYMBOLS

q	free stream dynamic pressure = $(\rho_\infty V_\infty^2)/2$
r	local radius of model
u, v, w	velocities in boundary-layer coordinates
x	surface coordinate in longitudinal direction
y, Y	coordinate perpendicular to local surface
z	cylindrical coordinate along model axis
A	reference area = $\pi D^2/4$
C_{DBL}	viscous drag = $(\iint \tau_x \cos\theta_B dS)/qA$
C_{DF}	total drag = $(\iint p_w \sin\theta_B dS)/qA$ + CDBL
$C_{\ell p}$	roll damping = $(\iint r\tau_\phi dS)/(qAD\ PD/V)$
C_m	pitching moment = $(\iint z p_w \cos\phi\cos\theta_B dS)/qAD$
$C_{M\alpha}$	slope of pitching moment coefficient = $dC_m/d\alpha$
$C_{M_{p\alpha}}$	slope of Magnus moment coefficient = $(dC_n/d\alpha)/(PD/V)$
$C_{M_q} + C_{M_{\dot\alpha}}$	pitch damping = $C_{n\dot\theta}/\sin\sigma$
C_N	normal force = $(\iint p_w \cos\phi\cos\theta_B dS)/qA$
C_n	Magnus moment = $[\iint (z p_w \sin\phi\cos\theta_B + z\tau_\phi \cos\phi\cos\theta_B + z\Delta p \sin\phi\cos\theta_B + z\tau_x \sin\phi\sin\theta_B) dS]/(qAD)$
$C_{n\dot\theta}$	side moment in coning motion = $(\iint (z-z_{cg}) p_w \sin\phi\cos\theta_B dS)/(qA\dot\theta)$
CP_N	center of pressure = C_m/C_N
CP_Y	Magnus center of pressure = C_n/C_Y
C_Y	Magnus force = $[\iint (p_w \sin\phi\cos\theta_B + \tau_\phi \cos\phi\cos\theta_B + \Delta p \sin\phi\cos\theta_B + \tau_x \sin\phi\sin\theta_B) dS]/qA$
D	diameter of model

LIST OF SYMBOLS
(CONTINUED)

LN	length of nose in calibers (shown as L1 in Figure 1)
P	spin rate, rad/s
Re_{ℓ}	Reynolds number based on model length
S	surface area
V	velocity along model trajectory
Δp	centrifugal pressure gradient contribution to side force
σ	effective angle of attack for coning motion
τ_x	longitudinal velocity wall shear
τ_ϕ	circumferential velocity wall shear
θ_B	local slope of body surface
$\dot{\theta}$	magnitude of the angular velocity of the shell
$\bar{\Omega}$	angular velocity of the body-fixed coordinates measured with respect to an inertial system

DISTRIBUTION LIST

No. of Copies	Organization
12	Commander Defense Technical Info Center ATTN: DDC-DDA Cameron Station Alexandria, VA 22314
1	Commander US Army Materiel Development and Readiness Command ATTN: DRCDMD-ST 5001 Eisenhower Avenue Alexandria, VA 22333
8	Commander US Army Armament Research and Development Command ATTN: DRDAR-TSS (2 cys) DRDAR-LCA-F Mr. D. Mertz Mr. E. Falkowski Mr. A. Loeb Mr. R. Kline Mr. S. Kahn Mr. S. Wasserman Dover, NJ 07801
1	Commander US Army Armament Materiel Readiness Command ATTN: DRSAR-LEP-L, Tech Lib Rock Island, IL 61299
1	Director US Army Armament Research and Development Command ATTN: DRDAR-LCB-TL Watervliet, NY 12189
1	Commander US Army Aviation Research and Development Command ATTN: DRDAV-E 4300 Goodfellow Blvd. St. Louis, MO 63120
1	Director US Army Air Mobility Research and Development Laboratory Ames Research Center Moffett Field, CA 94035
1	Commander US Army Communications Research and Development Command ATTN: DRDCO-PPA-SA Fort Monmouth, NJ 07703
1	Commander US Army Electronics Research and Development Command Technical Support Activity ATTN: DELSD-L Fort Monmouth, NJ 07703
3	Commander US Army Missile Command ATTN: DRSMI-R DRSMI-RDK Mr. R. Deep Mr. R. Becht Redstone Arsenal, AL 35809
1	Commander US Army Missile Command ATTN: DRSMI-YDL Redstone Arsenal, AL 35809
1	Commander US Army Tank Automotive Research and Development Command ATTN: DRDTA-UL Warren, MI 48090
1	Director US Army TRADOC Systems Analysis Activity ATTN: ATAA-SL, Tech Lib White Sands Missile Range, NM 88002

DISTRIBUTION LIST

No. of Copies	Organization
1	Commander US Army Research Office P. O. Box 12211 Research Triangle Park NC 27709
1	Commander US Naval Air Systems Command ATTN: AIR-604 Washington, D. C. 20360
2	Commander David W. Taylor Naval Ship Research and Development Center ATTN: Dr. S. de los Santos Mr. Stanley Gottlieb Bethesda, Maryland 20084
4	Commander US Naval Surface Weapons Center ATTN: Dr. T. Clare, Code DK20 Dr. P. Daniels Mr. D. A. Jones III Mr. L. Mason Dahlgren, VA 22448
4	Commander US Naval Surface Weapons Center ATTN: Code 312 Mr. R. Voisinet Mr. R. Driftmeyer Mr. J. Knott Mr. R. Schlie Silver Spring, MD 20910
1	Commander US Naval Weapons Center ATTN: Code 3431, Tech Lib China Lake, CA 93555
1	Director NASA Langley Research Center ATTN: NS-185, Tech Lib Langley Station Hampton, VA 23365
4	Director NASA Ames Research Center ATTN: MS-202A-14 Dr. P. Kutler MS-202-1, Dr. T. Pulliam MS-227-8, Dr. L. Schiff MS-202, Tech Lib Moffett Field, CA 94035
1	Nielsen Engineering & Research, Inc. ATTN: Dr. S. Stahara 510 Clyde Avenue Mountain View, CA 94043
2	Sandia Laboratories Aeroballistics Division 5631 ATTN: G.R. Eisner H.R. Vaughn Albuquerque, NJ 87184
1	Massachusetts Institute of Technology ATTN: Tech Library 77 Massachusetts Avenue Cambridge, MA 02139
1	Stanford University Department of Aeronautics and Astronautics ATTN: Prof. J. Steger Stanford, CA 94035
1	University of California, Davis Department of Mechanical Engineering ATTN: Prof. H.A. Dwyer Davis, CA 95616
1	University of Colorado Department of Aerospace Engineering ATTN: Prof. G. Inger Boulder, CO 80309

DISTRIBUTION LIST

No. of Copies	Organization
1	University of Delaware Mechanical and Aerospace Engineering Department ATTN: Dr. J. E. Danberg Newark, DE 19711
1	University of Florida ATTN: Dr. J.E. Milton P.O. Box 1918 Eglin AFB, FL 32542
1	Virginia Polytechnic Institute and State University Department of Aerospace and Oceanic Engineering ATTN: Prof. C. Lewis Blacksburg, VA 24061

Aberdeen Proving Ground

Dir, USAMSAA
ATTN: DRXSY-D
DRXSY-MP, H. Cohen

Cdr, USATECOM
ATTN: DRSTE-TO-F

Dir, USACSL, Bldg. E3516, EA
ATTN: DRDAR-CLB-PA

USER EVALUATION OF REPORT

Please take a few minutes to answer the questions below; tear out this sheet, fold as indicated, staple or tape closed, and place in the mail. Your comments will provide us with information for improving future reports.

1. BRL Report Number _____

2. Does this report satisfy a need? (Comment on purpose, related project, or other area of interest for which report will be used.)

_____

_____

_____

3. How, specifically, is the report being used? (Information source, design data or procedure, management procedure, source of ideas, etc.) _____

_____

_____

4. Has the information in this report led to any quantitative savings as far as man-hours/contract dollars saved, operating costs avoided, efficiencies achieved, etc.? If so, please elaborate.

_____

_____

5. General Comments (Indicate what you think should be changed to make this report and future reports of this type more responsive to your needs, more usable, improve readability, etc.) _____

_____

_____

_____

6. If you would like to be contacted by the personnel who prepared this report to raise specific questions or discuss the topic, please fill in the following information.

Name: _____

Telephone Number: _____

Organization Address: _____

_____

_____